electrocardiogram using a cardiotachometer. Esophageal temperature of the animal, measured using a thermometer (CTM-303; TERUMO), was maintained at ~37°C using a heating pad and a lamp. Both vagal nerves were exposed and sectioned bilaterally through a midline cervical incision. With the animal in the lateral position, we resected the left fifth and sixth ribs to approach the heart. After the incision of the pericardium, the heart was suspended in a pericardial cradle. Stainless steel wires were attached to the apex and the posterior wall of the left ventricle to pace the heart. Using a fine guiding needle, we implanted a dialysis probe transversely through the anterolateral free wall of the left ventricle. Next, we attached a pair of bipolar platinum electrodes to the cardiac end of each sectioned vagal nerve. The nerves and electrodes were covered in warmed mineral oil for insulation. We gave heparin sodium (100 U/kg) intravenously to prevent blood coagulation. At the end of the experiment, postmortem examination confirmed that the semipermeable membrane of the dialysis probe had been implanted in the left ventricular myocardium.

Dialysis Technique

The materials and properties of the dialysis probe have been described previously (1). Briefly, we designed a transverse dialysis probe in which a dialysis fiber of semipermeable membrane (13 mm length, 310 μm outer diameter, 200 μm inner diameter; PAN-1200, 50,000 mol wt cutoff; Asahi Chemical) was attached at both ends to polyethylene tubes (25 cm length, 500 μm outer diameter, 200 μm inner diameter). The dialysis probe was perfused at a rate of 2 μl/min with Ringer solution containing the cholinesterase inhibitor physostigmine (100 μM). Experimental protocols were started 2 h after implanting the dialysis probe when the ACh concentration in the dialysate reached a steady state. ACh concentrations in the dialysate were measured by an HPLC system with electrochemical detection (Eicom, Kyoto, Japan).

Figure 1 schematizes the three original protocols and two supplemental protocols utilized in the present study. The hatched rectangle indicates the baseline sampling, whereas the solid rectangles indicate the sampling during the 10-min vagal stimulation period (1 ms, 10 V, 20 Hz) in each protocol. The stimulus was set supramaximal to most easily delineate the possible effect of ANG II on myocardial interstitial ACh release. In all of the vagal stimulation periods, we paced the heart at 200 beats/min to avoid the difference in heart rate affecting the vagal stimulation-induced ACh release (14). For baseline sampling periods, we paced the heart at 200 beats/min when spontaneous heart rate was <200 beats/min.

Protocol 1 ($n = 6$). We examined the effects of intravenous administration of ANG II on vagal stimulation-induced myocardial ACh release. We collected a dialysate sample under baseline conditions. We then stimulated the vagal nerve and paced the heart for 10 min and collected a dialysate sample during the stimulation period

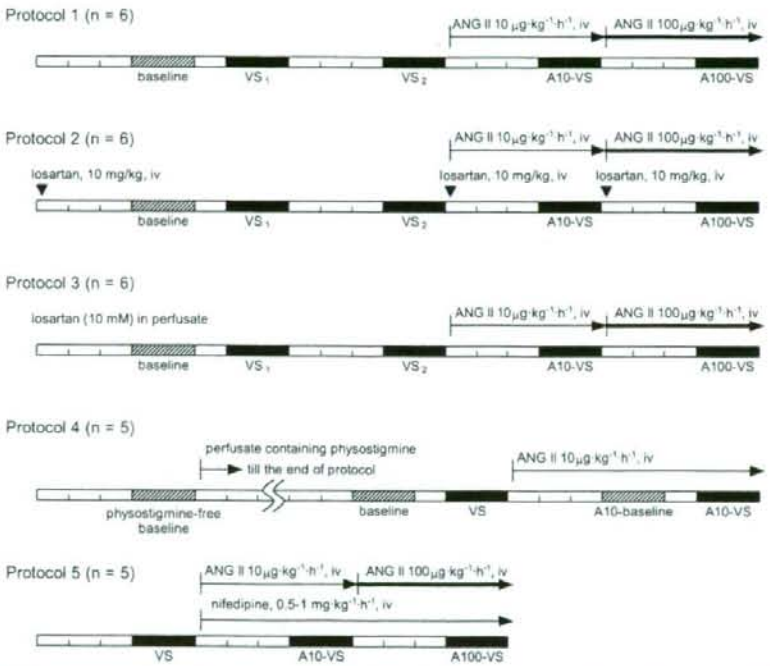

Fig. 1. Schematic representation of the protocols used in the present study. After implantation of the dialysis probe (2 h), we obtained a baseline dialysate sample (hatched rectangles) for 10 min. Thereafter, we obtained 4 dialysate samples during vagal stimulation with fixed-rate pacing for 10 min (filled rectangles) at intervening intervals of 15 min. In *protocols 1* through *3*, after obtaining 2 control trials (VS_1 and VS_2), we initiated intravenous administration of ANG II at 10 $\mu g \cdot kg^{-1} \cdot h^{-1}$ and waited for 15 min to obtain a dialysate sample during vagal stimulation with fixed-rate pacing (A10-VS). We then increased the dose of ANG II to 100 $\mu g \cdot kg^{-1} \cdot h^{-1}$ and waited for an additional 15 min before obtaining a dialysate sample during vagal stimulation with fixed-rate pacing (A100-VS). In *protocol 2*, the ANG II receptor subtype 1 blocker losartan was administered by bolus injection (10 mg/kg) before obtaining a baseline dialysate sample and also immediately before the beginning of each dose of ANG II administration (▼). In *protocol 3*, we administered losartan (10 mM) through the dialysis probe throughout the protocol. In *protocol 4*, we first collected a dialysate sample using perfusate free of physostigmine. We then replaced the perfusate with Ringer solution containing physostigmine and collected dialysate samples of baseline and vagal stimulation (VS). Approximately 15 min after the onset of iv ANG II administration at 10 $\mu g \cdot kg^{-1} \cdot h^{-1}$, we collected dialysate samples of baseline (A10-baseline) and vagal stimulation (A10-VS). In *protocol 5*, we collected dialysate samples during a control vagal stimulation (VS) and during the 2 doses of iv ANG II administration (A10-VS and A100-VS). The pressor effect of ANG II was counteracted by simultaneous iv infusion of the L-type Ca^{2+} channel blocker nifedipine.

(VS_1). After an intervening interval of 15 min, we repeated the 10-min vagal stimulation with fixed-rate pacing and collected another dialysate sample (VS_2). After performing these two control trials, we began intravenous administration of ANG II at 10 $\mu g \cdot kg^{-1} \cdot h^{-1}$. Approximately 15 min after the onset of the ANG II administration, we collected a dialysate sample (A10-VS) during 10-min vagal stimulation with fixed-rate pacing. We then increased the dose of ANG II at 100 $\mu g \cdot kg^{-1} \cdot h^{-1}$. Approximately 15 min after the onset of the higher-dose ANG II administration, we collected a final dialysate sample (A100-VS) during 10-min vagal stimulation with fixed-rate pacing.

Protocol 2 (n = 6). We examined whether the intravenous AT_1 receptor antagonist losartan would block the effects of ANG II on the vagal stimulation-induced myocardial ACh release. We infused losartan potassium intravenously at 10 mg/kg and waited for ~15 min. We then collected baseline, VS_1, and VS_2 samples with an intervening interval of 15 min, as described in *protocol 1*. Next, after an additional bolus injection of losartan potassium at 10 mg/kg, we began intravenous infusion of ANG II at 10 $\mu g \cdot kg^{-1} \cdot h^{-1}$. After ~15 min, we obtained a dialysate sample of A10-VS. Finally, after another bolus injection of losartan potassium at 10 mg/kg, we began intravenous infusion of ANG II at 100 $\mu g \cdot kg^{-1} \cdot h^{-1}$. After an additional 15 min, we obtained a dialysate sample of A100-VS.

Protocol 3 (n = 6). We examined whether local administration of losartan would block the effects of ANG II on the vagal stimulation-induced myocardial ACh release. We perfused the dialysis probe with Ringer solution containing 10 mM of losartan potassium. Taking into account the distribution across the semipermeable membrane, we administered losartan at a concentration >400 times higher than that for intravenous administration in *protocol 2*. Because local administrations of larger molecules such as ω-conotoxin GVIA (molecular weight 3037) and ω-conotoxin MVIIC (mol wt 2,749) were able to suppress vagal stimulation-induced ACh release in our previous study (15), it would be reasonable to assume that losartan potassium (mol wt 461) should have spread in the vicinity of the dialysis fiber, from which the dialysate was collected. Using the same procedures as described in *protocol 1*, we obtained dialysate samples for baseline, VS_1, VS_2, A10-VS, and A100-VS. A previous study indicated that ACh measured by cardiac microdialysis in the left ventricle mainly reflected ACh released from the postganglionic nerve terminals and not from the parasympathetic ganglia (1 and see DISCUSSION for details).

Protocol 4 (n = 5). To examine the effects of ANG II on the baseline ACh level, we performed an additional protocol where the baseline ACh level was measured during intravenous infusion of ANG II at 10 $\mu g \cdot kg^{-1} \cdot h^{-1}$ (A10-baseline). In this protocol, we also obtained a dialysate sample using the perfusate without the cholinesterase inhibitor physostigmine before the usual dialysate sampling using the perfusate containing physostigmine.

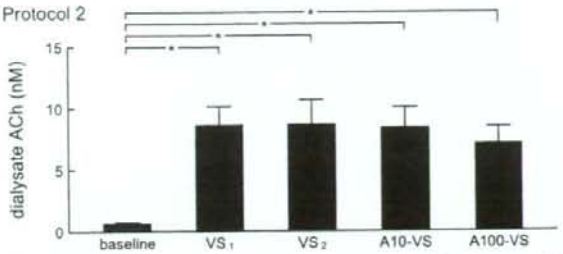

Fig. 3. Changes in dialysate ACh concentrations obtained from *protocol 2*. Vagal stimulation significantly increased the ACh levels. There was no significant difference in the ACh level among the 4 dialysate samples during vagal stimulation (VS_1, VS_2, A10-VS, and A100-VS). Values are presented as means and SE. *$P < 0.01$ by Tukey's test.

Protocol 5 (n = 5). To avoid the pressor effect of ANG II, we administered an L-type Ca^{2+} channel blocker nifedipine (0.5–2.0 $mg \cdot kg^{-1} \cdot h^{-1}$) simultaneously with ANG II and obtained dialysate samples for VS, A10-VS, and A100-VS. In a previous study, intravenous administration of an L-type Ca^{2+} channel blocker alone did not affect the vagal stimulation-induced myocardial ACh release significantly (15).

Statistical Analysis

All data are presented as mean ± SE values. In *protocols 1* through *3*, myocardial interstitial ACh levels were compared among baseline, VS_1, VS_2, A10-VS, and A100-VS samples using a repeated-measures ANOVA (8). When there was a significant difference, Tukey's test for all-pairwise comparisons was applied to identify the differences between any two of the samples. Differences were considered significant at $P < 0.05$. The mean AP value in the last 1 min of the 10-min vagal stimulation period was treated as the AP value during vagal stimulation. The AP data were compared using a repeated-measures ANOVA among baseline, during the two control stimulations (VS_1 and VS_2), and before and during vagal stimulation under the two different doses of intravenous ANG II administrations. When there was a significant difference, Dunnett's test for comparison against a single control was applied to identify differences from the baseline value. Differences were considered significant at $P < 0.05$. In

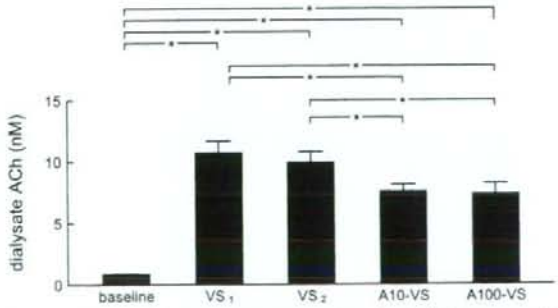

Fig. 2. Changes in dialysate ACh concentrations obtained from *protocol 1*. Vagal stimulation significantly increased the ACh levels. There was no significant difference in the ACh level between the 2 control trials (VS_1 and VS_2). The ACh level was significantly lower in A10-VS and A100-VS compared with that measured in VS_1 and VS_2. There was no significant difference in the ACh level between A10-VS and A100-VS. Values are presented as mean and SE. *$P < 0.01$ by Tukey's test.

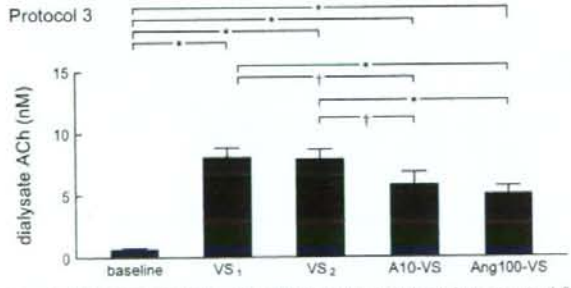

Fig. 4. Changes in dialysate ACh concentrations obtained from *protocol 3*. Vagal stimulation significantly increased the ACh levels. There was no significant difference in the ACh level between the 2 control trials (VS_1 and VS_2). The ACh level was significantly lower in A10-VS and A100-VS compared with that measured in VS_1 and VS_2. There was no significant difference in the ACh level between A10-VS and A100-VS. Values are presented as means and SE. †$P < 0.05$ and *$P < 0.01$ by Tukey's test.

Table 1. *Mean arterial pressure values before vagal stimulation and during the last 1 min of stimulation*

	Baseline	VS_1	VS_2	A10	A10-VS	A100	A100-VS
Protocol 1	102±11	93±17	91±17	132±9†	105±19	129±13†	105±21
Protocol 2	102±17	71±16*	69±16*	80±15	68±17*	86±19	72±18*
Protocol 3	102±13	100±17	92±17	139±11*	120±19	147±11*	122±21

Data are means ± SE obtained from baseline, two control trials (VS_1 and VS_2), before (A10) and during (A10-VS) vagal stimulation under iv administration of ANG II at 10 $\mu g \cdot kg^{-1} \cdot h^{-1}$, and before (A100) and during (A100-VS) vagal stimulation under iv administration of ANG II at 100 $\mu g \cdot kg^{-1} \cdot h^{-1}$. The heart was paced at 200 beats/min whenever vagal stimulation was applied. †$P < 0.05$ and *$P < 0.01$ from the respective baseline values by Dunnett's test.

protocol 4, the baseline ACh levels were compared before and during the ANG II administration using a paired *t*-test. The ACh levels during vagal stimulation were also compared before and during ANG II administration using a paired *t*-test. In *protocol 5*, the ACh levels and the mean AP values were compared among VS, A10-VS, and A100-VS using a repeated-measures ANOVA followed by Tukey's test.

RESULTS

In *protocol 1*, vagal stimulation significantly increased myocardial interstitial ACh levels (Fig. 2). There was no significant difference between two control trials with an intervening interval of 15 min [VS_1: 10.7 ± 1.0 (SE) nM and VS_2: 9.9 ± 0.9 (SE) nM]. Intravenous administration of ANG II at 10 $\mu g \cdot kg^{-1} \cdot h^{-1}$ significantly attenuated the vagal stimulation-induced ACh release (A10-VS: 7.5 ± 0.6 nM) to ~71% of VS_1. Although the intravenous administration of ANG II at 100 $\mu g \cdot kg^{-1} \cdot h^{-1}$ also significantly attenuated the vagal stimulation-induced ACh release (A100-VS: 7.3 ± 0.9 nM) to ~68% of VS_1, the ACh levels were not different from those of A10-VS.

In *protocol 2*, vagal stimulation significantly increased myocardial interstitial ACh levels under control stimulations (VS_1: 8.6 ± 1.5 nM and VS_2: 8.7 ± 2.0 nM; Fig. 3). With a pretreatment of intravenous losartan, intravenous ANG II was unable to suppress the vagal stimulation-induced ACh release (A10-VS: 8.4 ± 1.7 nM and A100-VS: 7.1 ± 1.4 nM). Although the mean level of ACh tended to be lower in A100-VS compared with VS_1 or VS_2, the differences were not statistically significant.

In *protocol 3*, vagal stimulation significantly increased myocardial interstitial ACh levels under control stimulations (VS_1: 8.0 ± 0.8 nM and VS_2: 7.9 ± 0.8 nM; Fig. 4). Intravenous ANG II at either 10 $\mu g \cdot kg^{-1} \cdot h^{-1}$ or 100 $\mu g \cdot kg^{-1} \cdot h^{-1}$ significantly suppressed the vagal stimulation-induced ACh release to ~72% (A10-VS: 5.8 ± 1.0 nM) and 62% (A100-VS: 5.0 ± 0.7 nM of that seen in VS_1), respectively.

In *protocol 1*, the AP values before the vagal stimulation during the intravenous ANG II administrations (A10 and A100) were significantly higher than the baseline AP value (Table 1). The AP values during vagal stimulation (VS_1, VS_2, A10-VS, and A100-VS) were not different from the baseline AP value. In *protocol 2*, the AP value before the first administration of losartan was 126 ± 14 mmHg. The AP values before the vagal stimulation during the intravenous ANG II administrations (A10 and A100) were not significantly different from the baseline AP value. The AP values during vagal stimulation (VS_1, VS_2, A10-VS, and A100-VS) were significantly lower than the baseline AP value. In *protocol 3*, the AP values before vagal stimulation during the intravenous ANG II administrations (A10 and A100) were significantly higher than the baseline AP value. The AP values during vagal stimulation (VS_1, VS_2, A10-VS, and A100-VS) did not differ statistically from the baseline AP value.

Figure 5 illustrates typical chromatograms obtained from one animal in *protocol 4*. The baseline ACh level was below the limit of determination (0.5 nM) when the perfusate did not contain physostigmine. Approximately 1 h after replacing the perfusate with Ringer solution containing physostigmine, the baseline ACh level was above the limit of determination. As shown in Table 2, vagal stimulation significantly increased the ACh level (VS). The intravenous administration of ANG II did not affect the baseline ACh level (A10-basline) but significantly attenuated the ACh level during vagal stimulation (A10-VS).

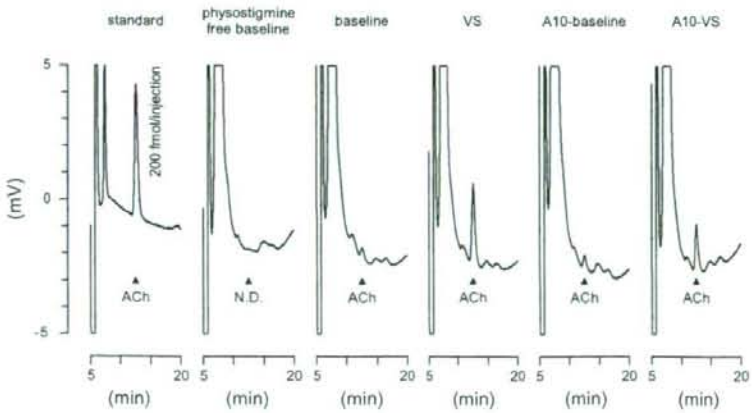

Fig. 5. Typical chromatograms for the ACh measurements obtained from *protocol 4*. ACh was less than the limit of determination when perfusate did not contain physostigmine (physostigmine-free baseline). The baseline ACh level was above the limit of determination when perfusate contained 100 μM physostigmine. (This perfusate was usually used for the ACh measurements.) Vagal stimulation increased the ACh level (VS). The administration of ANG II at 10 $\mu g \cdot kg^{-1} \cdot h^{-1}$ did not affect baseline ACh level (A10-baseline) but significantly attenuated the vagal stimulation-induced ACh release (A10-VS). See Table 2 for pooled data of ACh levels. ND, not detected.

Table 2. *Mean arterial pressure values and ACh concentrations obtained in protocol 4*

	Physostigmine-free Baseline	Baseline	VS	A10-Baseline	A10-VS
ACh, nM	Not detected	1.6±0.4	10.6±2.4	1.7±0.5	7.8±2.1*
Mean arterial pressure, mmHg	111±11	109±12	103±6	148±3*	118±6

Data are means ± SE obtained from physostigmine-free baseline, baseline, control vagal stimulation (VS), and baseline (A10-baseline) and vagal stimulation (A10-VS) under iv administration of ANG II at 10 $\mu g \cdot kg^{-1} \cdot h^{-1}$. There was no significant difference in the ACh level between baseline and A10-baseline by a paired-*t*-test. The ACh level was significantly lower in A10-VS than in VS by a paired-*t*-test. Mean arterial pressure was significantly higher in A10-baseline compared with the physostigmine-free baseline value by Dunnett's test. *$P < 0.01$.

In *protocol 5*, the pressor effect of ANG II was counteracted by the simultaneous intravenous infusion of nifedipine (Table 3). Under this condition, the intravenous administration of ANG II significantly attenuated the stimulation-induced ACh level to ~83% (A10-VS) and 72% (A100-VS) of that seen in VS.

DISCUSSION

The present study demonstrated that intravenous ANG II significantly inhibited the vagal stimulation-induced myocardial interstitial ACh release in the left ventricle in anesthetized cats. Intravenous administration of losartan abolished the inhibitory effect of ANG II on the stimulation-induced ACh release, suggesting that the inhibitory action of ANG II was mediated by AT_1 receptors.

Inhibitory Effect of ANG II on Myocardial Interstitial ACh Release

Only a few reports have focused on the modulatory effects of ANG II on the parasympathetic nervous system (3, 5, 25, 26), all of which have used the heart rate reduction in response to vagal stimulation as a functional measurement to assess the peripheral vagal function. Although ANG II has been shown to inhibit the ACh release in the rat entorhinal cortex in vitro (4), the direct evidence for the inhibitory effect of ANG II on the ACh release in the peripheral vagal neurotransmission in vivo has been lacking. The present study demonstrated that intravenous ANG II inhibited the vagal nerve stimulation-induced ACh release in the left ventricle in vivo (Fig. 2). As for the sympathetic system in the heart, Lameris et al. (18) have previously demonstrated that ANG II does not affect the sympathetic nerve stimulation-induced norepinephrine release. The insignificant effect of ANG II on the sympathetic neurotransmission and the inhibitory effect of ANG II on the parasympathetic neurotransmission may provide the basis for a study by Takata et al. (26) in which ACE inhibitor enhanced cardiac vagal but not sympathetic neurotransmission.

Table 3. *Mean arterial pressure values and ACh concentrations obtained in protocol 5*

	VS	A10-VS	A100-VS
ACh, nM	12.7±1.1	10.6±1.1†	9.2±1.5*
Mean arterial pressure, mmHg	83.4±12.2	68.4±6.3	70.4±9.5

Data are means ± SE from a control vagal stimulation trial (VS), during vagal stimulation under iv administration of ANG II at 10 $\mu g \cdot kg^{-1} \cdot h^{-1}$ (A10-VS) and during vagal stimulation under iv administration of ANG II at 100 $\mu g \cdot kg^{-1} \cdot h^{-1}$ (A100-VS). The heart was paced at 200 beats/min during vagal stimulation. In this protocol, the pressor effect of ANG II was counteracted by simultaneous iv administration of the L-type Ca^{2+} channel blocker nifedipine (0.5–2 $mg \cdot kg^{-1} \cdot h^{-1}$). †$P < 0.05$ and *$P < 0.01$ from the VS group by Tukey's test. There was no significant difference between A10-VS and A100-VS in the ACh level. There were no significant differences in mean arterial pressure among the three trials.

An increased activity of the renin-angiotensin system is common in chronic heart failure and has been considered to be a stimulus for aggravation of the disease. Inhibition of the renin-angiotensin system by ACE inhibitors or by AT_1 receptor blockers can prevent the ventricular remodeling and improve the survival rate (16, 17), suggesting that ANG II is indeed involved in the aggravation of heart failure. ACh, on the other hand, can exert a cardioprotective effect against myocardial ischemia in several experimental settings (12, 24, 29). If ANG II inhibits the peripheral vagal neurotransmission, blockade of ANG II would increase the vagal effect on the heart. Actually, Du et al. (5) demonstrated that losartan enhanced bradycardia induced by vagal stimulation in rats with chronic myocardial infarction. In that study, however, the ventricular effect of vagal stimulation was not assessed. The results of the present study indicate that ANG II inhibited the vagal neurotransmission in the ventricle. Blockade of ANG II is therefore expected to increase the vagal effect on the ventricular myocardium when the vagal outflow from the central nervous system is unchanged. Although no literatures appear to be available as to the chronic effect of ACh on the prognosis of heart failure, electrical vagal stimulation was able to improve the survival rate of chronic heart failure in rats (19). In that study, the magnitude of the vagal stimulation was such that the heart rate decreased only by 20–30 beats/min in rats, suggesting that a modest increase in vagal tone would be sufficient to produce a cardioprotective effect. It is plausible that blockade of ANG II yields beneficial effects on chronic heart failure not only by antagonizing the sympathetic effects but also by enhancing the vagal effects on the ventricle.

Vagal stimulation was able to reduce the left ventricular contractility as assessed by end-systolic elastance only when sympathetic stimulation coexisted (20), suggesting that the effect of vagal stimulation on ventricular contractility would be secondary to sympathoinhibition. Accordingly, contribution of the inhibitory effect of ANG II on the stimulation-induced ACh release to the physiological regulation of ventricular contractility might be marginal. We think that the finding is important as a peripheral mechanism of vagal withdrawal in heart diseases accompanying the activation of the renin-angiotensin system.

Possible Site of the Inhibitory Action of ANG II on ACh Release

In *protocol 3*, we examined whether local administration of losartan was able to nullify the inhibitory effect of ANG II on the vagal stimulation-induced ACh release. The utility of local administration of pharmacological agents through the dialysis fiber has been confirmed previously. As an example, local administration the Na^+ channel inhibitor tetrodotoxin through the dialysis fiber completely blocked the nerve stimulation-induced ACh release (14). With respect to the source for ACh, intravenous administration of the nicotinic antagonist hexamethonium bromide completely blocked the stimulation-induced ACh release, whereas local administration of hexamethonium bromide did not, suggesting the lack of parasympathetic ganglia in the vicinity of dialysis fiber (1). In support of our interpretation, a neuroanatomic finding indicates that three ganglia, away from the left anterior free wall targeted by the dialysis probe, provide the major source of left ventricular postganglionic innervation in cats (11). Therefore, the myocardial interstitial ACh measured by cardiac microdialysis in the left ventricle mainly reflects the ACh release from the postganglionic vagal nerve terminals. The results of *protocol 3* indicate that losartan spread around the postganglionic vagal nerve terminals failed to abolish the inhibitory effect of ANG II on the stimulation-induced ACh release. Because intravenous administration of losartan was able to abolish the inhibitory effect of ANG II on the stimulation-induced ACh release (*protocol 2*), the site of this inhibitory action is likely at parasympathetic ganglia rather than at postganglionic vagal nerve terminals. The fact that AT_1 receptors are rich in parasympathetic ganglia (2) would support our interpretation.

ANG II has a direct vasoconstrictive effect on the coronary artery (30). At the same time, however, the intravenous administration of ANG II tended to increase mean AP during vagal stimulation by ~15 mmHg in *protocol 1* (Table 1). Although it was statistically insignificant, if this increase in mean AP increased cardiac oxygen demand, the coronary blood flow might have been increased (27), resulting in an increased rate of washout in the myocardial tissue. The possibility cannot be ruled out that such a washout mechanism contributed to the reduction of stimulation-induced ACh release during ANG II administration. However, the baseline ACh level was not decreased by ANG II in *protocol 4*, suggesting that the washout rate did not increase significantly. In addition, even when the pressor effect of ANG II was counteracted by nifedipine, ANG II was still able to inhibit the vagal stimulation-induced ACh release in *protocol 5*. Therefore, we think that the change in washout rate was not a principal mechanism for the reduction of stimulation-induced ACh release by ANG II.

The mechanisms for the baseline ACh release under the vagotomized condition were not identified in the present study. In the motor nerve terminals, a so-called nonquantal release of ACh is documented, which is independent of nerve activity (6). Incorporation of the vesicular transport system in the membrane of the nerve terminals during an exocytosis process is considered to be responsible for the mechanism of nonquantal ACh release. A similar mechanism might contribute to the baseline ACh release in the vagal nerve terminals.

Several limitations need to be addressed. First, the dose of ANG II might have increased the plasma ANG II concentration beyond the physiological range. In this regard, the observed effect might be rather pharmacological or pathological than physiological. Nevertheless, because there are local synthesis and degradation of ANG II in the heart (21, 28), the inhibition of ACh release by ANG II could operate locally in the heart. Second, whether ANG II inhibited the ACh release from the preganglionic nerve terminals or it suppressed the excitability of the postganglionic nerve fibers to ACh was not identified in the present study. Third, the involvement of ANG II receptor subtype 2 (AT_2 receptor) in the modulation of peripheral parasympathetic neurotransmission was not examined in the present study because intravenous losartan was able to abolish the inhibitory effect of ANG II on the stimulation-induced ACh release. However, if coactivation of AT_1 and AT_2 receptors is required for the inhibitory effect of ANG II, blockade of AT_2 receptors would also abolish the inhibitory effect. Forth, we tested just one level of vagal stimulation. Whether the effect of ANG II on the stimulation-induced ACh release depends on the vagal stimulation intensity remains to be resolved.

In conclusion, intravenous ANG II reduced the vagal nerve stimulation-induced ACh release in the left ventricle. Intravenous losartan abolished the inhibitory effect of ANG II on the stimulation-induced ACh release, suggesting that this inhibition was mediated by AT_1 receptors. Because local administration of losartan via dialysis fiber was unable to nullify the inhibitory effect of ANG II on the stimulation-induced ACh release, the site of this inhibitory action is likely parasympathetic ganglia. The present results imply that the beneficial effects of ACE inhibitors and AT_1 receptor antagonists in the treatment of heart diseases may include not only the suppression of sympathetic activity but also the enhancement of vagal activity to the ventricle.

GRANTS

This study was supported by a Health and Labour Sciences Research Grant for Research on Advanced Medical Technology, a Health and Labour Sciences Research Grant for Research on Medical Devices for Analyzing, Supporting, and Substituting the Function of Human Body, and Health and Labour Sciences Research Grant H18-Iryo-Ippan-023 from the Ministry of Health, Labour, and Welfare of Japan.

REFERENCES

1. **Akiyama T, Yamazaki T, Ninomiya I.** In vivo detection of endogenous acetylcholine release in cat ventricles. *Am J Physiol Heart Circ Physiol* 266: H854–H860, 1994.
2. **Allen AM, Zhuo J, Mendelsohn FA.** Localization and function of angiotensin AT_1 receptors. *Am J Hypertens* 13: 31S–38S, 2000.
3. **Andrews PL, Dutia MB, Harris PJ.** Angiotensin II does not inhibit vagally-induced bradycardia or gastric contractions in the anaesthetized ferret. *Br J Pharmacol* 82: 833–837, 1984.
4. **Barnes JM, Barnes NM, Costall B, Horovitz ZP, Naylor RJ.** Angiotensin II inhibits the release of [^{3}H]acetylcholine from rat entorhinal cortex in vitro. *Brain Res* 491: 136–143, 1989.
5. **Du XJ, Cox HS, Dart AM, Esler MD.** Depression of efferent parasympathetic control of heart rate in rats with myocardial infarction: effect of losartan. *J Cardiovasc Pharmacol* 31: 937–944, 1998.
6. **Edwards C, Doležal V, Tuček S, Zemková H, Vyskočil F.** Is an acetylcholine transport system responsible for nonquantal release of acetylcholine at the rodent myoneural junction? *Proc Natl Acad Sci USA* 82: 3354–3518, 1985.
7. **Gao L, Wang W, Li Y, Schultz HD, Liu D, Cornish KG, Zucker IH.** Sympathoexcitation by central ANG II: roles for AT_1 receptor upregulation and NAD(P)H oxidase in RVLM. *Am J Physiol Heart Circ Physiol* 288: H2271–H2279, 2005.
8. **Glantz SA.** *Primer of Biostatistics* (5th ed.). New York: McGraw-Hill, 2002.

9. **Hirooka Y, Head GA, Potts PD, Godwin SJ, Bendle RD, Dampney RA.** Medullary neurons activated by angiotensin II in the conscious rabbit. *Hypertension* 27: 287–296, 1996.
10. **Hughes J, Roth RH.** Evidence that angiotensin enhances transmitter release during sympathetic nerve stimulation. *Br J Pharmacol* 41: 239–255, 1971.
11. **Johnson TA, Gray AL, Lauenstein JM, Newton SS, Massari VJ.** Parasympathetic control of the heart. *I.* An interventriculo-septal ganglion is the major source of the vagal intracardiac innervation of the ventricles. *J Appl Physiol* 96: 2265–2272, 2004.
12. **Kakinuma Y, Ando M, Kuwabara M, Katare RG, Okudela K, Kobayashi M, Sato T.** Acetylcholine from vagal stimulation protects cardiomyocytes against ischemia and hypoxia involving additive non-hypoxic induction of HIF-1alpha. *FEBS Lett* 579: 2111–2118, 2005.
13. **Kawada T, Yamazaki T, Akiyama T, Sato T, Shishido T, Inagaki M, Takaki H, Sugimachi M, Sunagawa K.** Differential acetylcholine release mechanisms in the ischemic and non-ischemic myocardium. *J Mol Cell Cardiol* 32: 405–414, 2000.
14. **Kawada T, Yamazaki T, Akiyama T, Shishido T, Inagaki M, Uemura K, Miyamoto T, Sugimachi M, Takaki H, Sunagawa K.** In vivo assessment of acetylcholine-releasing function at cardiac vagal nerve terminals. *Am J Physiol Heart Circ Physiol* 281: H139–H145, 2001.
15. **Kawada T, Yamazaki T, Akiyama T, Uemura K, Kamiya A, Shishido T, Mori H, Sugimachi M.** Effects of Ca^{2+} channel antagonists on nerve stimulation-induced and ischemia-induced myocardial interstitial acetylcholine release in cats. *Am J Physiol Heart Circ Physiol* 291: H2187–H2191, 2006.
16. **Konstam MA, Neaton JD, Poole-Wilson PA, Pitt B, Segal R, Sharma D, Dasbach EJ, Carides GW, Dickstein K, Riegger G, Camm AJ, Martinez FA, Bradstreet DC, Ikeda LS, Santoro EP, investigators ELITEII.** Comparison of losartan and captopril on heart failure-related outcomes and symptoms from the losartan heart failure survival study (ELITE II). *Am Heart J* 150: 123–131, 2005.
17. **Konstam MA, Rousseau MF, Kronenberg MW, Udelson JE, Melin J, Stewart D, Dolan N, Edens TR, Ahn S, Kinan D, Howe DM, Kilcoyne L, Metherall J, Benedict C, Yusuf S, Pouleur H, investigators SOLVD.** Effects of the angiotensin converting enzyme inhibitor enalapril on the long-term progression of left ventricular dysfunction in patients with heart failure. *Circulation* 86: 431–438, 1992.
18. **Lameris TW, de Zeeuw S, Duncker DJ, Alberts G, Boomsma F, Verdouw PD, van den Meiracker AH.** Exogenous angiotensin II does not facilitate norepinephrine release in the heart. *Hypertension* 40: 491–497, 2002.
19. **Li M, Zheng C, Sato T, Kawada T, Sugimachi M, Sunagawa K.** Vagal nerve stimulation markedly improves long-term survival after chronic heart failure in rats. *Circulation* 109: 120–124, 2004.
20. **Nakayama Y, Miyano H, Shishido T, Inagaki M, Kawada T, Sugimachi M, Sunagawa K.** Heart rate-independent vagal effect on end-systolic elastance of the canine left ventricle under various levels of sympathetic tone. *Circulation* 104: 2277–2279, 2001.
21. **Paul M, Mehr AP, Kreutz R.** Physiology of local renin-angiotensin systems. *Physiol Rev* 86: 747–803, 2006.
22. **Peach MJ.** Renin-angiotensin system: Biochemistry and mechanisms of action. *Physiol Rev* 57: 313–370, 1977.
23. **Potter EK.** Angiotensin inhibits action of vagus nerve at the heart. *Br J Pharmacol* 75: 9–11, 1982.
24. **Qin Q, Downey JM, Cohen MV.** Acetylcholine but not adenosine triggers preconditioning through PI3-kinase and a tyrosine kinase. *Am J Physiol Heart Circ Physiol* 284: H727–H734, 2003.
25. **Rechtman M, Majewski H.** A facilitatory effect of anti-angiotensin drugs on vagal bradycardia in the pithed rat and guinea-pig. *Br J Pharmacol* 110: 289–296, 1993.
26. **Takata Y, Arai T, Suzuki S, Kurihara J, Uezono T, Okubo Y, Kato H.** Captopril enhances cardiac vagal but not sympathetic neurotransmission in pithed rats. *J Pharmacol Sci* 95: 390–393, 2004.
27. **Tune JD, Gorman MW, Feigl EO.** Matching coronary blood flow to myocardial oxygen consumption. *J Appl Physiol* 97: 404–415, 2004.
28. **van Kats JP, Danser AH, van Meegen JR, Sassen LM, Verdouw PD, Schalekamp MA.** Angiotensin production by the heart. A quantitative study in pigs with the use of radiolabeled angiotensin infusions. *Circulation* 98: 73–81, 1998.
29. **Yao Z, Gross GJ.** Acetylcholine mimics ischemic preconditioning via a glibenclamide-sensitive mechanism in dogs. *Am J Physiol Heart Circ Physiol* 264: H2221–H2225, 1993.
30. **Zhang C, Knudson JD, Setty S, Araiza A, Dincer üD, Kuo L, Tune JD.** Coronary arteriolar vasoconstriction to angiotensin II is augmented in prediabetic metabolic syndrome via activation of AT_1 receptors. *Am J Physiol Heart Circ Physiol* 288: H2154–H2162, 2005.

Am J Physiol Heart Circ Physiol 293: H1564–H1570, 2007.
First published May 25, 2007; doi:10.1152/ajpheart.00368.2007.

Muscarinic potassium channels augment dynamic and static heart rate responses to vagal stimulation

Masaki Mizuno,[1] Atsunori Kamiya,[1] Toru Kawada,[1] Tadayoshi Miyamoto,[1,2,3] Shuji Shimizu,[1,2] and Masaru Sugimachi[1]

[1]*Department of Cardiovascular Dynamics, Advanced Medical Engineering Center, National Cardiovascular Center Research Institute, and* [3]*Morinomiya University of Medical Sciences, Osaka; and* [2]*Japan Association for the Advancement of Medical Equipment, Tokyo, Japan*

Submitted 23 March 2007; accepted in final form 22 May 2007

Mizuno M, Kamiya A, Kawada T, Miyamoto T, Shimizu S, Sugimachi M. Muscarinic potassium channels augment dynamic and static heart rate responses to vagal stimulation. *Am J Physiol Heart Circ Physiol* 293: H1564–H1570, 2007. First published May 25, 2007; doi:10.1152/ajpheart.00368.2007.—Vagal control of heart rate (HR) is mediated by direct and indirect actions of ACh. Direct action of ACh activates the muscarinic K^+ (K_{ACh}) channels, whereas indirect action inhibits adenylyl cyclase. The role of the K_{ACh} channels in the overall picture of vagal HR control remains to be elucidated. We examined the role of the K_{ACh} channels in the transfer characteristics of the HR response to vagal stimulation. In nine anesthetized sinoaortic-denerved and vagotomized rabbits, the vagal nerve was stimulated with a binary white-noise signal (0–10 Hz) for examination of the dynamic characteristic and in a step-wise manner (5, 10, 15, and 20 Hz/min) for examination of the static characteristic. The dynamic transfer function from vagal stimulation to HR approximated a first-order, low-pass filter with a lag time. Tertiapin, a selective K_{ACh} channel blocker (30 nmol/kg iv), significantly decreased the dynamic gain from 5.0 ± 1.2 to 2.0 ± 0.6 (mean ± SD) beats·min^{-1}·Hz^{-1} ($P < 0.01$) and the corner frequency from 0.25 ± 0.03 to 0.06 ± 0.01 Hz ($P < 0.01$) without changing the lag time (0.37 ± 0.04 vs. 0.39 ± 0.05 s). Moreover, tertiapin significantly attenuated the vagal stimulation-induced HR decrease by 46 ± 21, 58 ± 18, 65 ± 15, and 68 ± 11% at stimulus frequencies of 5, 10, 15, and 20 Hz, respectively. We conclude that K_{ACh} channels contribute to a rapid HR change and to a larger decrease in the steady-state HR in response to more potent tonic vagal stimulation.

systems analysis; transfer function; muscarinic receptor; rabbit

VAGAL CONTROL OF HEART RATE (HR) is mediated by a cascade reaction to ACh release. ACh binds to M_2 muscarinic receptors and, consequently, decreases HR. However, the pathway is not simple; two different pathways mediate the ACh-induced HR decrease. The M_2 muscarinic receptors activate heterotrimeric G_i and/or G_o proteins in cardiac myocytes (18); the action of ACh is determined by the G_i protein subunits. Via a direct pathway, a G_i protein βγ-subunit activates inwardly rectifying muscarinic K^+ (K_{ACh}) channels in the sinoatrial node cells (11, 28, 35); K_{ACh} channels then exert a negative chronotropic effect by hyperpolarizing the sinoatrial node cells. On the other hand, via an indirect pathway, a G_i protein α-subunit suppresses adenylyl cyclase (12, 32); the suppression of adenylyl cyclase then decreases HR by inhibiting inward currents in the sinoatrial node cells, which are activated by cAMP or cAMP-dependent protein kinase. However, functional roles of the direct and indirect actions of ACh are not fully understood in the overall picture of vagal control of HR.

As a function in the dual control of adenylyl cyclase by G protein (12), the indirect action of ACh counteracts the G_s proteins activated by β_1-adrenergic sympathetic stimulation and relies on slower changes in intracellular cAMP levels (8). On the contrary, the direct action of ACh utilizes the faster membrane-delimited mechanisms involving K_{ACh} channels (3) and is believed to be independent of sympathetic control. Given the rapidity of vagal HR control compared with sympathetic control (2, 14, 31), we hypothesized that the direct action of ACh via K_{ACh} channels contributes to the quickness of the vagal HR control in vivo. To test this hypothesis, we used the selective K_{ACh} channel blocker tertiapin to examine the dynamic and static transfer characteristics of the HR response to vagal stimulation (7, 10, 13, 15).

The pioneering work by Yamada (34) demonstrated that the direct action of ACh via K_{ACh} channels mediates ~75% of the steady-state negative chronotropic effects relative to the maximum carbachol-induced bradycardia in the isolated rabbit heart (i.e., static HR response to vagal stimulation). However, in this study, the role of K_{ACh} channels in the dynamic HR response to vagal stimulation was not analyzed quantitatively. Because HR changes dynamically in response to daily activities, quantification of dynamic and static characteristics is equally important. For instance, information on the dynamic HR response is key to understanding the generation of HR variability. Berger et al. (2) used transfer function analysis to identify the dynamic characteristics of the HR response. Saul et al. (29) demonstrated the utility of transfer function analysis for insight into cardiovascular regulation. The present study aims to expand our knowledge of the involvement of K_{ACh} channels in dynamic HR control by the vagal system.

MATERIALS AND METHODS

Surgical preparations. Animal care was consistent with the "Guiding Principles for Care and Use of Animals in the Field of Physiological Sciences," of the Physiological Society of Japan. All protocols were reviewed and approved by the Animal Subjects Committee of the National Cardiovascular Center. Nine Japanese White rabbits (2.5–3.2 kg body wt) were anesthetized by a mixture of urethane (250 mg/ml) and α-chloralose (40 mg/ml): initiation with a bolus injection of 2 ml/kg and maintenance with continuous administration at 0.5

Address for reprint requests and other correspondence: M. Mizuno, Dept. of Cardiovascular Dynamics, Advanced Medical Engineering Center, National Cardiovascular Center Research Institute, 5-7-1 Fujishirodai, Suita, Osaka 565-8565, Japan (e-mail: m-mizuno@ri.ncvc.go.jp).

The costs of publication of this article were defrayed in part by the payment of page charges. The article must therefore be hereby marked "*advertisement*" in accordance with 18 U.S.C. Section 1734 solely to indicate this fact.

$ml \cdot kg^{-1} \cdot h^{-1}$. The rabbits were intubated and mechanically ventilated with oxygen-enriched room air. Arterial pressure (AP) was measured by a micromanometer (model SPC-330A, Millar Instruments, Houston, TX) inserted into the right femoral artery and advanced to the thoracic aorta. HR was measured with a cardiotachometer (model N4778, San-ei, Tokyo, Japan). A double-lumen catheter was introduced into the right femoral vein for continuous anesthetic and drug administration. Sinoaortic denervation was performed bilaterally to minimize changes in the sympathetic efferent nerve activity via arterial baroreflexes. Bilateral section of the cardiac postganglionic sympathetic nerves minimized any possible interaction between the vagus and sympathetic nerves. The vagi were sectioned bilaterally at the neck. A pair of bipolar electrodes were attached to the cardiac end of the sectioned right vagus for vagal stimulation. Immersion of the stimulation electrodes and nerves in a mixture of white petroleum jelly (Vaseline) and liquid paraffin prevented drying and provided insulation. Body temperature was maintained at 38°C with a heating pad throughout the experiment.

Experimental procedures. The pulse duration of nerve stimulation was set at 2 ms. The stimulation amplitude of the right vagus was adjusted to yield an HR decrease of ~50 beats/min at a stimulation frequency of 10 Hz. After this adjustment, the amplitude of vagal stimulation was fixed at 1.8–6.0 V. Initiation of vagal nerve stimulation over 1 h upon completion of surgical preparations allowed stable hemodynamics. A preliminary examination indicated that the response of HR to vagal stimulation was stable for up to 3 h in our experimental settings (10 min of dynamic vagal stimulation at 50-min intervals; data not shown).

Dynamic protocol. For estimation of the dynamic transfer characteristics from vagal stimulation to HR response, the right vagus was stimulated by a frequency-modulated pulse train for 10 min. The stimulation frequency was switched every 500 ms at 0 or 10 Hz according to a binary white-noise signal. The power spectrum of the stimulation signal was reasonably constant up to 1 Hz. The transfer function was estimated up to 1 Hz, because the reliability of estimation decreased as a result of the diminution of input power above this frequency. The selected frequency range sufficiently spanned the physiological range of interest with respect to the dynamic vagal control of HR.

Static protocol. For estimation of the static transfer characteristics from vagal stimulation to HR response, step-wise vagal stimulation was performed. Vagal stimulation frequency was increased from 5 to 20 Hz in 5-Hz increments. Each frequency step was maintained for 60 s.

The dynamic and static transfer functions from vagal stimulation to HR response were estimated under control and K_{ACh} channel blockade conditions. After the control data were recorded, a bolus injection (30 nmol/kg iv) of a selective K_{ACh} channel blocker, tertiapin (Peptide Institute, Osaka, Japan), was administered, and vagal stimulation protocols were repeated 15 min thereafter. The control data were obtained first in all animals, because the long-lasting (>2 h) effects of tertiapin (data not shown) did not permit the subsequent acquisition of control data. A >5-min interval between dynamic and step-wise stimulation protocols confirmed that AP and HR returned to baseline levels. Dynamic and step-wise vagal stimulation protocols were randomly assigned under control and K_{ACh} channel blockade conditions.

β-Adrenergic blockade protocol. A supplemental experiment was performed under β-adrenergic blockade ($n = 3$) eliminated any effect of sympathetic activity. At ~10 min after a bolus injection of propranolol (1 mg/kg iv) (22), HR and AP reached a new steady state. The dynamic and static transfer functions from vagal stimulation to HR response were estimated before and after tertiapin treatment, both under β-adrenergic blockade.

Data analysis. A 12-bit analog-to-digital converter was used to digitize data at 200 Hz, and data were stored on the hard disk of a dedicated laboratory computer system. The dynamic transfer function from binary white-noise vagal stimulation to HR response was estimated as follows. Input-output data pairs of the vagal stimulation frequency and HR were resampled at 10 Hz; then data pairs were partitioned into eight 50%-overlapping segments consisting of 1,024 data points each. For each segment, the linear trend was subtracted, and a Hanning window was applied. A fast Fourier transform was then performed to obtain the frequency spectra for vagal stimulation [$N(f)$] and HR [$HR(f)$] (4). Over the eight segments, the power of vagal stimulation [$S_{N \cdot N}(f)$], the power of HR [$S_{HR \cdot HR}(f)$], and the cross power between these two signals [$S_{N \cdot HR}(f)$] were ensemble averaged. Finally, the transfer function [$H(f)$] from vagal stimulation to the HR response was determined as follows (1, 20)

$$H(f) = \frac{S_{N \cdot HR}(f)}{S_{N \cdot N}(f)} \tag{1}$$

The transfer function from vagal stimulation to HR response approximated a first-order, low-pass filter with a lag time in previous studies (14, 21–24); therefore, the estimated transfer function was parameterized as follows

$$H(f) = \frac{-K}{1 + \frac{f}{f_c} j} e^{-2\pi f L} \tag{2}$$

where K represents the dynamic gain (or, more precisely, the steady-state gain, in $beats \cdot min^{-1} \cdot Hz^{-1}$), f_c denotes the corner frequency (in Hz), L denotes the lag time (in s), and f and j represent frequency and the imaginary unit, respectively. The negative sign in the numerator indicates the negative HR response to vagal stimulation. The steady-state gain indicates the asymptotic value of the relative amplitude of the HR response to vagal nerve stimulation obtained in the frequency of input modulation approaching zero. The corner frequency represents the frequency of input modulation at which gain decreases by 3 dB from the steady-state gain in the frequency domain and reflects the readiness of the HR response for vagal stimulation in the time domain. The dynamic gain, corner frequency, and lag time were estimated by an iterative nonlinear least-squares regression. The phase shift of the transfer function indicates, with respect to the input signal, a lag or lead in the output signal normalized by its corresponding frequency of input modulation.

To quantify the linear dependence of the HR response on vagal stimulation, the magnitude-squared coherence function [$Coh(f)$] was estimated as follows (1, 20)

$$Coh(f) = \frac{|S_{N \cdot HR}(f)|^2}{S_{N \cdot N}(f) \cdot S_{HR \cdot HR}(f)} \tag{3}$$

Coherence values range from zero to unity. Unity coherence indicates perfect linear dependence between the input and output signals; in contrast, zero coherence indicates total independence between the two signals.

To facilitate the intuitive understanding of the system dynamic characteristics, we calculated the system step response of HR to 1-Hz nerve stimulation as follows. The system impulse response was derived from the inverse Fourier transform of $H(f)$. The system step response was then obtained from the time integral of the impulse response. The length of the step response was 51.2 s. We calculated the maximum step response by averaging the last 10 s of the step response. The 90% rise time of the step response was determined as the time required for the response to reach 90% of the maximum step response. The time constant of the step response was calculated from the corner frequency of the corresponding transfer function as follows

$$\text{time constant} = \frac{1}{2 \cdot \pi \cdot fc} \tag{4}$$

where the time constant is related inversely to the corner frequency without influence of the lag time.

The static transfer function from step-wise vagal stimulation to HR was estimated by averaging the HR data during the final 10 s of the 60-s stimulation at each stimulation frequency.

Statistical analysis. Values are means ± SD. Student's paired *t*-test was used to test differences in fitted parameters and calculated step response between control and K_{ACh} channel blockade conditions. For hemodynamic parameters, a two-way ANOVA, with drug and vagal stimulation as the main effects, was used to determine significant differences. For percent reduction from the control conditions in each parameter, one-way ANOVA was used to determine significant differences. $P < 0.05$ was considered significant.

RESULTS

Dynamic characteristics. Figure 1*A* shows typical recordings and corresponding power spectra of vagal stimulation and HR response under control and K_{ACh} channel blockade conditions. Random vagal stimulation decreased HR intermittently. Tertiapin-mediated K_{ACh} channel blockade attenuated the amplitude of the variation and the speed of the HR response to vagal stimulation. In the power spectral plot, tertiapin decreased the HR power. The decrease in the HR power was

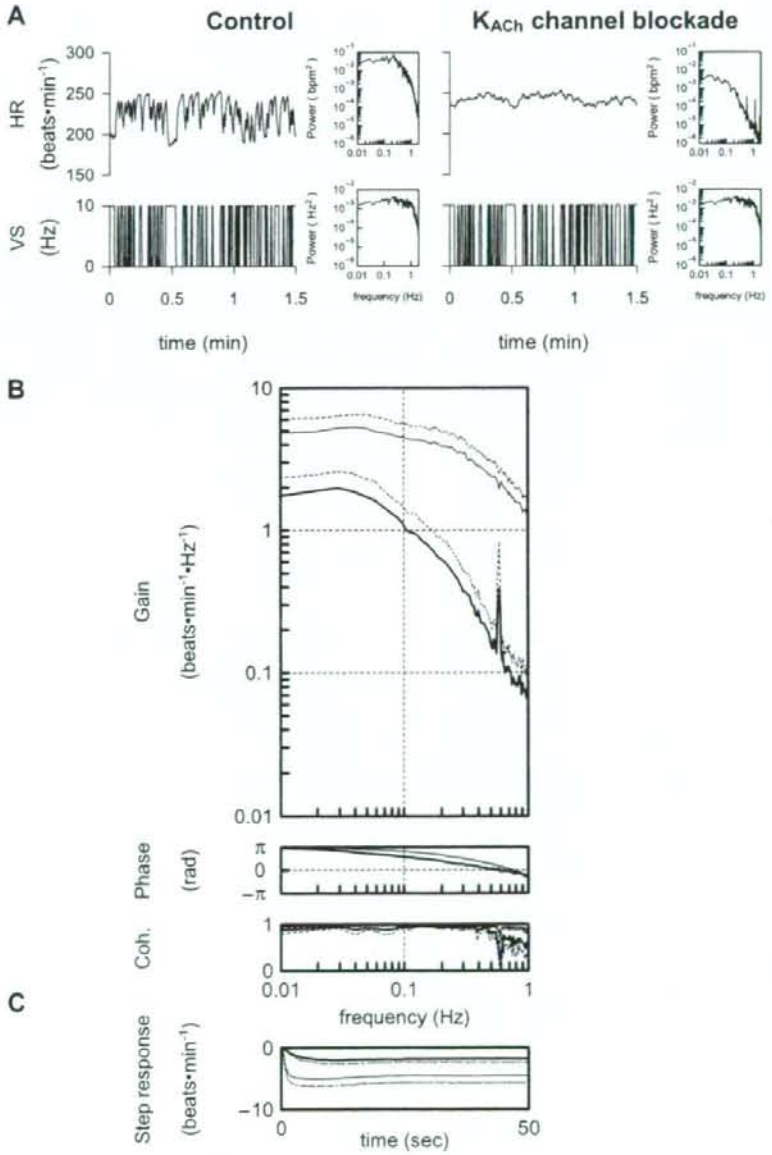

Fig. 1. *A*: representative recordings of heart rate (HR) obtained utilizing binary white-noise vagal stimulation (*top*) and corresponding vagal stimulation (VS, *bottom*). Traces were recorded before (control, *left*) and after tertiapin infusion (30 nmol/kg iv) for muscarinic K^+ (K_{ACh}) channel blockade (*right*). *Insets*: power spectra of each parameter. Tertiapin attenuated amplitude of HR variation and speed of response of HR to vagal stimulation. *B*: dynamic transfer function relating vagal stimulation to HR responses averaged from all animals (pooled data, $n = 9$). *Top*: gains; *middle*: phase shifts; *bottom*: coherence (Coh) functions. Frequency on abscissa (gain and phase) indicates frequency of input modulation, rather than stimulation frequency. *C*: calculated step response to 1-Hz tonic vagal stimulation averaged from all animals (pooled data, $n = 9$). Solid lines, means; dashed lines, SD. Thin line, control; thick line, K_{ACh} channel blockade with tertiapin (30 nmol/kg iv). Tertiapin decreased transfer gain and increased phase shift with increasing frequency, and tertiapin decreased maximum step response and slowed initial step response.

Table 1. *Effects of tertiapin infusion on AP and HR before and during dynamic vagal stimulation*

	Control	Tertiapin
AP, mmHg		
Before stimulation	82.4±20.5	77.6±20.7
During stimulation	77.9±20.0	74.8±18.6
HR, beats/min		
Before stimulation	247.3±24.7	248.1±32.7
During stimulation	212.4±22.3	231.1±25.9

Values are means ± SD (n = 9). Tertiapin was infused at 30 nmol/kg iv. AP, arterial pressure; HR, heart rate. Vagal stimulation significantly decreased HR ($P < 0.01$), but no significant effect of drug ($P = 0.28$) or interaction ($P = 0.32$) was observed by 2-way ANOVA.

more potent in the higher (>0.1 Hz) than in the lower frequency range.

Table 1 summarizes the mean values of AP and HR before and during vagal stimulation averaged from all animals. Dynamic vagal stimulation significantly decreased the mean HR ($P < 0.01$), but not the mean AP. Tertiapin did not significantly affect mean AP or HR before or during stimulation.

Figure 1*B* illustrates the dynamic transfer functions characterizing the vagal HR response averaged from all animals under control and tertiapin-mediated K_{ACh} channel blockade conditions. Gain plots, phase plots, and coherence functions are shown. Tertiapin attenuated the dynamic gain compared with the control conditions; the extent of the attenuation was greater in the higher frequency range: 63.0 ± 11.6, 74.4 ± 8.3, 93.0 ± 2.5, and 93.3 ± 3.9% at 0.01. 0.1, 0.5, and 1 Hz, respectively, as normalized to the control condition ($P < 0.01$ by ANOVA). The peak in the gain at 0.6 Hz observed during tertiapin-mediated K_{ATP} channel blockade would be caused by the artificial respiration (respiratory rate = 35–40 min^{-1}), because the low coherence value (~0.1) at 0.6 Hz indicates the independence of the input and output signals. This peak was masked by the large HR response to vagal stimulation under the control condition. The phase approached π radians at the lowest frequency and lagged with increasing frequency under the control condition; tertiapin caused the phase difference between the two conditions in the frequency range of 0.03–0.7 Hz, which disappeared at 1 Hz. The fitted parameters of the transfer functions are summarized in Table 2. Tertiapin significantly decreased the dynamic gain and the corner frequency without changing the lag time. Coherence was near unity in the overall frequency range in the control condition, whereas a decrease in the coherence function from unity was noted at >0.6 Hz with K_{ACh} channel blockade.

Figure 1*C* shows the calculated step response of HR to vagal stimulation averaged from all animals in the control condition and during K_{ACh} channel blockade. Tertiapin slowed the transient response (time constants = 0.6 ± 0.1 to 2.7 ± 0.5 s, $P < 0.01$) and attenuated the HR response to vagal stimulation (maximum step response = −4.5 ± 1.2 to −1.8 ± 0.6 beats/min, $P < 0.01$) in the time domain. Furthermore, tertiapin significantly delayed the 90% rise time of the step response, which was calculated as an index of system readiness (1.6 ± 0.5 to 5.0 ± 1.4 s, $P < 0.01$).

Static characteristics. Figure 2*A* shows typical recordings of step-wise vagal stimulation and the HR response in the control condition and during K_{ACh} channel blockade. The step-wise vagal stimulation decreased HR in a step-wise manner. Tertiapin attenuated the static reductions of HR from the baseline HR.

Figure 2*B* summarizes changes in HR in response to step-wise vagal stimulation. The step-wise vagal stimulation significantly decreased HR with increasing stimulus frequency under both conditions. Tertiapin significantly attenuated the static reductions of HR. The attenuation of HR reduction normalized to control conditions increased with increasing stimulus frequency: 45.8 ± 21.3, 58.2 ± 17.9, 64.7 ± 14.6, and 68.0 ± 11.4% at 5, 10, 15, and 20 Hz, respectively ($P < 0.05$ by ANOVA).

β-Adrenergic blockade protocol. In the supplemental protocol (n = 3) with β-adrenergic blockade, tertiapin decreased the dynamic gain from 2.4 ± 0.6 to 1.3 ± 0.5 beats·min^{-1}·Hz^{-1} and the corner frequency from 0.23 ± 0.05 to 0.06 ± 0.02 Hz without changing the lag time (0.36 ± 0.01 vs. 0.43 ± 0.00 s). In terms of the static characteristics, tertiapin significantly attenuated the vagal stimulation-induced HR decrease by 43 ± 10, 50 ± 8, 56 ± 7, and 61 ± 8% at stimulus frequencies of 5, 10, 15, and 20 Hz, respectively.

DISCUSSION

We have quantified the role of the K_{ACh} channels by examining the transfer characteristics. The major findings in the present study are that K_{ACh} channel blockade with intravenous tertiapin administration decreased the dynamic gain and corner frequency without changing the lag time of the dynamic transfer function from vagal stimulation to HR. These findings support our hypothesis that direct action of ACh via K_{ACh} channels contributes to the quickness of the HR control in response to electrical vagal stimulation.

Effect of tertiapin on dynamic transfer characteristics. Our results indicate that K_{ACh} channels contribute to a rapid component in vagal HR control. Tertiapin slowed the dynamic HR response to vagal stimulation, since tertiapin attenuated the gain of the transfer function significantly in the high frequency range (Fig. 1*B*). Moreover, the calculated step response clearly demonstrated this point (Fig. 1*C*). Tertiapin prolonged the time constant and 90% rise time of the step response by 2.1 and 3.4 s, respectively. Since quickness is a hallmark of the vagal control of HR relative to sympathetic control, these results highlight the importance of K_{ACh} channels in the rapidity of vagal HR control. Because tertiapin did not affect the lag time (Table 2), the increase in the 90% rise time to the step response due to tertiapin (~3.4 s) may primarily reflect the slowed transient response.

Our results are consistent with and may partly explain the earlier studies in which transgenic mice were used to investigate the role of K_{ACh} channels (8, 33). Using the G protein-

Table 2. *Effects of tertiapin infusion on parameters of the transfer function relating dynamic vagal stimulation to HR*

	Control	Tertiapin
Dynamic gain, beats·min^{-1}·Hz^{-1}	5.0±1.2	2.0±0.6*
Corner frequency, Hz	0.25±0.03	0.06±0.01*
Lag time, s	0.37±0.04	0.39±0.05

Values are means ± SD. Tertiapin was infused at 30 nmol/kg iv. *$P < 0.01$ vs. corresponding control.

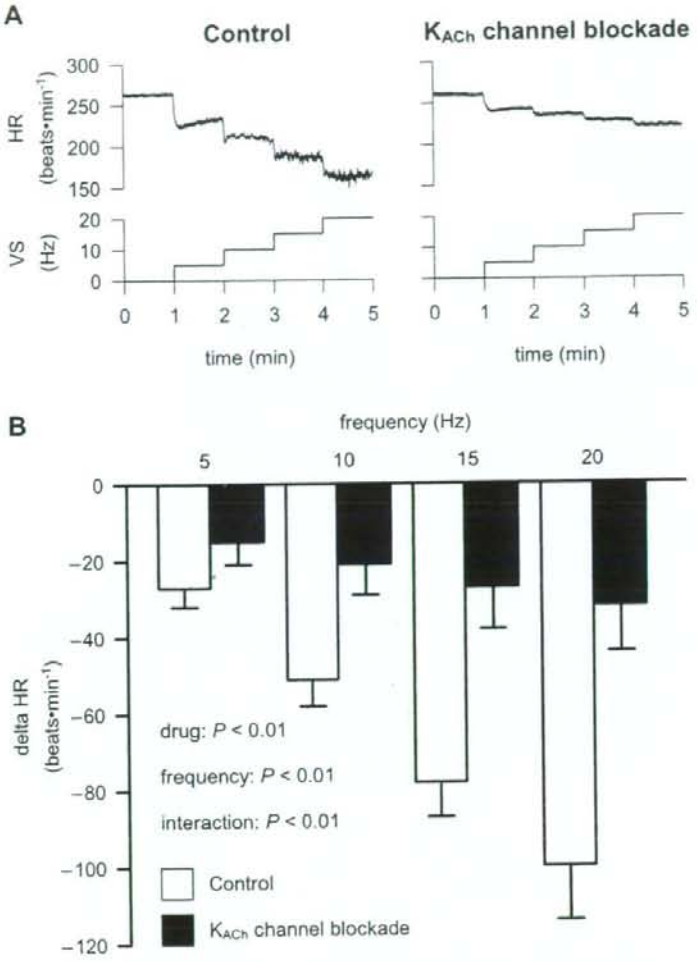

Fig. 2. *A*: representative recordings of HR (*top*) and corresponding vagal stimulation (*bottom*) obtained utilizing a step-wise stimulation. Traces were recorded before (control, *left*) and after tertiapin infusion (30 nmol/kg iv) for K_{ACh} channel blockade (*right*). K_{ACh} channel blockade attenuated amplitude of HR variation to tonic vagal stimulation. *B*: static transfer function relating step-wise vagal stimulation to HR responses averaged from all animals (pooled data, $n = 9$). Basal HR was not different between control and K_{ACh} channel blockade (see Table 1). K_{ACh} channel blockade decreases static HR response, and static reductions in bradycardic effect were greater at higher stimulation frequencies.

gated inwardly rectifying potassium (GIRK) channel family subunit GIRK4, which is a component of K_{ACh} channels (5, 16), Wickman et al. (33) indicated that the spectral power of HR was lower at 1.5–5.0 Hz, which is predominantly vagally mediated, but not at <0.4 Hz, in GIRK4-knockout than in wild-type mice. Another study using transgenic mice with a reduction in functional βγ-subunits of the G_i proteins also showed impaired vagal HR control, such as reductions in carbachol-induced bradycardia, HR variability, and baroreflex sensitivity (8). In the present study, tertiapin significantly attenuated the dynamic gain compared with the control conditions in the frequency bands from 0.01 to 1 Hz; the extent of the decreases in dynamic gain was augmented with increasing frequency of input modulation. This finding also supports the notion that K_{ACh} channels play a large part as a rapid component of vagal control of HR. Furthermore, increased phase shift due to tertiapin in the higher frequency range (0.03–0.7 Hz) would support the interpretation that the K_{ACh} channel current played an important role in the rapid HR response to vagal stimulation.

Tertiapin-mediated changes in fitted parameters of the transfer function from vagal stimulation to HR suggest that, at the postjunctional effector sites, the K_{ACh} channels play a key role in determining the dynamic properties of transduction from vagal nerve activity to HR. To quantitatively elucidate vagal and sympathetic control of HR, our research group used a transfer function analysis to examine the system characteristics. First, the transfer function from dynamic vagal nerve stimulation to HR approximated the characteristics of a first-order, low-pass filter, whereas the transfer function from dynamic sympathetic nerve stimulation to HR approximated the characteristics of a second-order, low-pass filter (14). Dynamic gain of vagal stimulation to HR was increased by concomitant sympathetic nerve stimulation (14) and pharmacologically induced accumulation of cAMP at the postjunctional effector sites (23) and decreased by high plasma norepinephrine (21). These perturbations of the indirect action of ACh did not affect the quickness of vagal HR control; i.e., neither corner frequency nor lag time was altered. On the contrary, inhibition of cholinesterase by neostigmine decreased the corner frequency

and increased the lag time (24). Taken together, these results might suggest that not only ACh kinetics at the neuroeffector site, but also the K_{ACh} channels at the postjunctional effector sites, play a key role in determining the dynamic properties of transduction from vagal nerve activity to HR.

Effect of tertiapin on the static transfer characteristics. Tertiapin attenuates the static reduction of HR in accord with the attenuation of the gain of the dynamic transfer function at the lowest frequency of input modulation. This suggests that K_{ACh} channels contribute to the static, as well as the rapid, component of vagal HR control. The relative attenuation of HR reduction increased with increasing stimulus frequency (Fig. 2*B*), suggesting that direct action of ACh in the static properties of transduction from vagus nerve activity to HR is augmented by an increase in the amount of available ACh. Although it is well established that the muscarinic response to static vagal stimulation depends on the stimulation frequency (26, 27), whether the contribution of the K_{ACh} channel pathway to the total HR response depends on the stimulus frequency remains unknown. The basal mean HR of GIRK-knockout mice (33) and transgenic mice with a reduction of βγ-subunits of the G_i proteins (8) is the same as that of wild-type mice, suggesting that K_{ACh} channels are not involved in mean HR control in the basal state. At low-to-moderate levels of vagal activity, vagal control of HR is due to changes in cAMP-modulated I_h, often referred to as "pacemaker" current (6). K_{ACh} channels might play an essential role in HR control at high levels of vagal activity.

In the present study, tertiapin decreased the HR response to vagal stimulation by ~70% of the control condition at a stimulus intensity of 20 Hz. This value is consistent with the earlier study by Yamada (34). This consistency suggested that K_{ACh} channels contribute to ~70% of the maximum negative chronotropic effects to pharmacologically and/or electronically induced vagal stimulation. However, changes in HR induced by tertiapin may have in turn affected the indirect action of ACh in the present study. Therefore, the percentage of direct vs. indirect action should be carefully interpreted.

Limitations. There are several limitations to this study. First, we did not confirm the completeness of K_{ACh} channel blockade. Kitamura et al. (15) demonstrated that tertiapin potently and selectively blocked the K_{ACh} channel in cardiac myocytes in a muscarinic receptor- and voltage-independent manner. Furthermore, Drici et al. (7) showed that tertiapin blocked K_{ACh} channels with an IC_{50} of ~30 nM with no significant effect on major currents associated with the cardiac repolarization process or atrioventricular conduction. On the basis of these studies, Hashimoto et al. (10) demonstrated that tertiapin (12 nmol/kg iv) significantly prolonged the atrial effective refractory period during vagal stimulation in their in vivo canine study. Therefore, we believe that the dose of tertiapin (30 nmol/kg iv) used in the present study should be sufficient to block K_{ACh} channel current in vivo.

Second, data were obtained from anesthetized animals. Since the anesthesia would affect the autonomic tone, the results may not be directly applicable to conscious animals. However, because we cut and stimulated the right cardiac vagal nerve, changes in autonomic outflow associated with anesthesia might not have significantly affected the results.

Third, in the present study, we stimulated the vagal nerve according to binary white noise and a step-wise pattern, which was quite different from the pattern of physiological neuronal discharge. However, although nonphysiological patterns of stimulation could theoretically bias the system identification results, because coherence was near unity over the frequency range of interest, by virtue of their inherent linearity, the system properties would not vary much with differing patterns of stimulation.

In conclusion, K_{ACh} channel blockade with intravenous tertiapin administration decreased the dynamic gain and corner frequency without changing the lag time of the transfer function from vagal stimulation to HR. In the time domain, tertiapin prolonged the time constant and 90% rise time of the step response. Additionally, tertiapin decreased the static reductions of HR from baseline HR to less than half of the control response with increasing vagal stimulus frequency. These results suggest that K_{ACh} channels accelerate the dynamic HR response to vagal stimulation and contribute more to the static HR response for more potent tonic vagal stimulation in vivo.

Perspectives

To simply identify the role of K_{ACh} channels in vagal HR control, a previous study (34) and the present study completely and/or partially excluded background sympathetic tone. However, in the physiological condition, sympathetic tone affects vagal control of HR and vice versa [e.g., accentuated antagonism (17)]. Pathophysiological conditions such as chronic heart failure (25), hypertension (19), and obesity (30) reveal increased basal sympathetic nerve activity compared with the normal condition. Tertiapin did not affect basal AP or HR (Table 1), suggesting that tertiapin did not affect sympathetic tone in the present experimental settings. Furthermore, under β-adrenergic blockade (the supplemental protocol), tertiapin decreased the dynamic gain and corner frequency, suggesting that the effects of tertiapin cannot be explained by the background sympathetic tone. However, the experimental design of the present study did not allow separate assessment of the direct vs. the indirect action of ACh, because the indirect action of ACh was not manipulated intentionally. Further investigation is needed to clarify the effects of sympathetic tone on the contribution of K_{ACh} channels to negative chronotropic effects.

GRANTS

This study was supported by Health and Labour Sciences Research Grants H15-Physi-001, H18-Nano-Ippan-003, and H18-Iryo-Ippan-023 from the Ministry of Health, Grant-in-Aid for Scientific Research promoted by the Ministry of Education, Culture, Sports, Science and Technology in Japan 18591992, and the Ground-Based Research Announcement for Space Utilization project promoted by the Japan Space Forum. This study was also supported by Industrial Technology Research Program Grant 06B44524a from the New Energy and Industrial Technology Development Organization of Japan.

REFERENCES

1. **Bendat J, Piersol A.** Single-input/output relationships. In: *Random Data Analysis and Measurement Procedures* (3rd ed). New York: Wiley, 2000, p. 189–217.
2. **Berger RD, Saul JP, Cohen RJ.** Transfer function analysis of autonomic regulation. I. Canine atrial rate response. *Am J Physiol Heart Circ Physiol* 256: H142–H152, 1989.
3. **Breitwieser GE, Szabo G.** Uncoupling of cardiac muscarinic and β-adrenergic receptors from ion channels by a guanine nucleotide analogue. *Nature* 317: 538–540, 1985.
4. **Brigham E.** FFT transform application. In: *The Fast Fourier Transform and Its Application.* Englewood Cliffs, NJ: Prentice-Hall, 1988, p. 167–203.

5. **Dascal N, Schreibmayer W, Lim NF, Wang W, Chavkin C, DiMagno L, Labarca C, Kieffer BL, Gaveriaux-Ruff C, Trollinger D, Lester HA, Davidson N.** Atrial G protein-activated K^+ channel: expression, cloning, and molecular properties. *Proc Natl Acad Sci USA* 90: 10235–10239, 1993.
6. **DiFrancesco D.** Cardiac pacemaker: 15 years of "new" interpretation. *Acta Cardiol* 50: 413–427, 1995.
7. **Drici MD, Diochot S, Terrenoire C, Romey G, Lazdunski M.** The bee venom peptide tertiapin underlines the role of $I_{K\ ACh}$ in acetylcholine-induced atrioventricular blocks. *Br J Pharmacol* 131: 569–577, 2000.
8. **Gehrmann J, Meister M, Maguire CT, Martins DC, Hammer PE, Neer EJ, Berul CI, Mende U.** Impaired parasympathetic heart rate control in mice with a reduction of functional G protein βγ-subunits. *Am J Physiol Heart Circ Physiol* 282: H445–H456, 2002.
9. **Hartzell HC, Mery PF, Fischmeister R, Szabo G.** Sympathetic regulation of cardiac calcium current is due exclusively to cAMP-dependent phosphorylation. *Nature* 351: 573–576, 1991.
10. **Hashimoto N, Yamashita T, Tsuruzoe N.** Tertiapin, a selective $I_{K\ ACh}$ blocker, terminates atrial fibrillation with selective atrial effective refractory period prolongation. *Pharmacol Res* 54: 136–141, 2006.
11. **Huang CL, Slesinger PA, Casey PJ, Jan YN, Jan LY.** Evidence that direct binding of Gβγ to the GIRK1 G protein-gated inwardly rectifying K^+ channel is important for channel activation. *Neuron* 15: 1133–1143, 1995.
12. **Irisawa H, Brown HF, Giles W.** Cardiac pacemaking in the sinoatrial node. *Physiol Rev* 73: 197–227, 1993.
13. **Jin W, Lu Z.** Synthesis of a stable form of tertiapin: a high-affinity inhibitor for inward-rectifier K^+ channels. *Biochemistry* 38: 14286–14293, 1999.
14. **Kawada T, Ikeda Y, Sugimachi M, Shishido T, Kawaguchi O, Yamazaki T, Alexander J Jr, Sunagawa K.** Bidirectional augmentation of heart rate regulation by autonomic nervous system in rabbits. *Am J Physiol Heart Circ Physiol* 271: H288–H295, 1996.
15. **Kitamura H, Yokoyama M, Akita H, Matsushita K, Kurachi Y, Yamada M.** Tertiapin potently and selectively blocks muscarinic K^+ channels in rabbit cardiac myocytes. *J Pharmacol Exp Ther* 293: 196–205, 2000.
16. **Krapivinsky G, Gordon EA, Wickman K, Velimirovic B, Krapivinsky L, Clapham DE.** The G-protein-gated atrial K^+ channel $I_{K\ ACh}$ is a heteromultimer of two inwardly rectifying K^+-channel proteins. *Nature* 374: 135–141, 1995.
17. **Levy MN.** Sympathetic-parasympathetic interactions in the heart. *Circ Res* 29: 437–445, 1971.
18. **Luetje CW, Tietje KM, Christian JL, Nathanson NM.** Differential tissue expression and developmental regulation of guanine nucleotide binding regulatory proteins and their messenger RNAs in rat heart. *J Biol Chem* 263: 13357–13365, 1988.
19. **Mancia G, Grassi G, Giannattasio C, Seravalle G.** Sympathetic activation in the pathogenesis of hypertension and progression of organ damage. *Hypertension* 34: 724–728, 1999.
20. **Marmarelis P, Marmarelis V.** The white noise method in system identification. In: *Analysis of Physiological Systems*. New York: Plenum, 1978, p. 131–221.
21. **Miyamoto T, Kawada T, Takaki H, Inagaki M, Yanagiya Y, Jin Y, Sugimachi M, Sunagawa K.** High plasma norepinephrine attenuates the dynamic heart rate response to vagal stimulation. *Am J Physiol Heart Circ Physiol* 284: H2412–H2418, 2003.
22. **Miyamoto T, Kawada T, Yanagiya Y, Inagaki M, Takaki H, Sugimachi M, Sunagawa K.** Cardiac sympathetic nerve stimulation does not attenuate dynamic vagal control of heart rate via α-adrenergic mechanism. *Am J Physiol Heart Circ Physiol* 287: H860–H865, 2004.
23. **Nakahara T, Kawada T, Sugimachi M, Miyano H, Sato T, Shishido T, Yoshimura R, Miyashita H, Inagaki M, Alexander J Jr, Sunagawa K.** Accumulation of cAMP augments dynamic vagal control of heart rate. *Am J Physiol Heart Circ Physiol* 275: H562–H567, 1998.
24. **Nakahara T, Kawada T, Sugimachi M, Miyano H, Sato T, Shishido T, Yoshimura R, Miyashita H, Sunagawa K.** Cholinesterase affects dynamic transduction properties from vagal stimulation to heart rate. *Am J Physiol Regul Integr Comp Physiol* 275: R541–R547, 1998.
25. **Negrao CE, Rondon MU, Tinucci T, Alves MJ, Roveda F, Braga AM, Reis SF, Nastari L, Barretto AC, Krieger EM, Middlekauff HR.** Abnormal neurovascular control during exercise is linked to heart failure severity. *Am J Physiol Heart Circ Physiol* 280: H1286–H1292, 2001.
26. **Parker P, Celler BG, Potter EK, McCloskey DI.** Vagal stimulation and cardiac slowing. *J Auton Nerv Syst* 11: 226–231, 1984.
27. **Priola DV, Cote I.** Differential sensitivity of the canine heart to acetylcholine and vagal stimulation. *Am J Physiol Heart Circ Physiol* 234: H460–H464, 1978.
28. **Sakmann B, Noma A, Trautwein W.** Acetylcholine activation of single muscarinic K^+ channels in isolated pacemaker cells of the mammalian heart. *Nature* 303: 250–253, 1983.
29. **Saul JP, Berger RD, Albrecht P, Stein SP, Chen MH, Cohen RJ.** Transfer function analysis of the circulation: unique insights into cardiovascular regulation. *Am J Physiol Heart Circ Physiol* 261: H1231–H1245, 1991.
30. **Seals DR, Bell C.** Chronic sympathetic activation: consequence and cause of age-associated obesity? *Diabetes* 53: 276–284, 2004.
31. **Spear JF, Moore EN.** Influence of brief vagal and stellate nerve stimulation on pacemaker activity and conduction within the atrioventricular conduction system of the dog. *Circ Res* 32: 27–41, 1973.
32. **Sunahara RK, Dessauer CW, Gilman AG.** Complexity and diversity of mammalian adenylyl cyclases. *Annu Rev Pharmacol Toxicol* 36: 461–480, 1996.
33. **Wickman K, Nemec J, Gendler SJ, Clapham DE.** Abnormal heart rate regulation in GIRK4 knockout mice. *Neuron* 20: 103–114, 1998.
34. **Yamada M.** The role of muscarinic K^+ channels in the negative chronotropic effect of a muscarinic agonist. *J Pharmacol Exp Ther* 300: 681–687, 2002.
35. **Yamada M, Inanobe A, Kurachi Y.** G protein regulation of potassium ion channels. *Pharmacol Rev* 50: 723–760, 1998.

Annals of Biomedical Engineering, Vol. 37, No. 1, January 2009 (© 2008) pp. 112–128
DOI: 10.1007/s10439-008-9599-4

Wavelet-Based System Identification of Short-Term Dynamic Characteristics of Arterial Baroreflex

KOJI KASHIHARA,[1,2] TORU KAWADA,[3] MASARU SUGIMACHI,[3] and KENJI SUNAGAWA[4]

[1]Hypertension and Stroke Research Laboratory, Royal North Shore Hospital, University of Sydney, Ground Floor, Building 10, Royal North Shore Hospital, St. Leonards, NSW 2065, Australia; [2]National Institute for Longevity Sciences, NCGG, 36-3 Gengo, Morioka-machi, Obu City, Aichi 474-8511, Japan; [3]Department of Cardiovascular Dynamics, National Cardiovascular Center Research Institute, 5-7-1 Fujishirodai, Suita, Osaka 565-8565, Japan; and [4]Department of Cardiovascular Medicine, Kyushu University, 3-1-1, Maidashi, Higashi-ku, Fukuoka 812-8582, Japan

(Received 1 February 2008; accepted 31 October 2008; published online 12 November 2008)

Abstract—The assessment of arterial baroreflex function in cardiovascular diseases requires quantitative evaluation of dynamic and static baroreflex properties because of the frequent modulation of baroreflex properties with unstable hemodynamics. The purpose of this study was to identify the dynamic baroreflex properties from transient changes of step pressure inputs with background noise during a short-duration baroreflex test in anesthetized rabbits with isolated carotid sinuses, using a modified wavelet-based time-frequency analysis. The proposed analysis was able to identify the transfer function of baroreflex as well as static properties from the transient input-output responses under normal [gain at 0.04 Hz from carotid sinus pressure (CSP) to arterial pressure ($n = 8$); 0.29 ± 0.05 at low (40–60 mmHg), 1.28 ± 0.12 at middle (80–100 mmHg), and 0.38 ± 0.07 at high (120–140 mmHg) CSP changes] and pathophysiological [gain in control vs. phenylbiguanide ($n = 8$); 0.32 ± 0.07 vs. 0.39 ± 0.09 at low, 1.39 ± 0.15 vs. 0.59 ± 0.09 ($p < 0.01$) at middle, and 0.35 ± 0.04 vs. 0.15 ± 0.02 ($p < 0.01$) at high CSP changes] conditions. Subsequently, we tested the proposed wavelet-based method under closed-loop baroreflex responses; the simulation study indicates that it may be applicable to clinical situations for accurate assessment of dynamic baroreflex function. In conclusion, the dynamic baroreflex property to various pressure inputs could be simultaneously extracted from the step responses with background noise.

Keywords—Baroreceptor reflex, Sympathetic nerve activity, Arterial pressure, Transfer function, Dynamic characteristics.

INTRODUCTION

Arterial baroreflex is a crucial negative feedback system because of the quick stabilization of arterial pressure (AP) against external pressure disturbances.[12,30] The assessment of arterial baroreflex function would require quantifying the dynamic as well as static properties[15,46] because the baroreflex gain or sensitivity is frequently modulated during cardiovascular diseases.[6,36,39] Because quick responses of autonomic nerves and AP mainly through the brainstem[3] might contain the unknown characteristics changing by the minute in acute cardiovascular diseases,[25] the short-term dynamic system identification might relate to the novel finding under such nonstationary condition. Laboratory and spontaneous baroreflex methods[37] are widely used in human and animal studies. The laboratory method requires invasive pharmacological or mechanical pressure interventions, and it may be suitable for estimation of the mechanism of AP regulation through the sympathetic as well as vagal baroreflex.[7,45] The spontaneous baroreflex method aims to assess cardiovagal activity noninvasively using systolic AP and heart rate variability.[5] These methods have various merits under the baroreflex testing conditions, but remain debatable because of complicated mechanisms.[27,37,40,43]

In the laboratory method, the standard analysis of sympathetic baroreflex has been performed mainly in the time[10,16] or frequency domain.[1,29,35,44] The time-domain analysis has evaluated the stable or maximal gain around the operating point, but may not characterize the impaired dynamic baroreflex properties accurately in cardiovascular patients with unstable hemodynamics and background noise. In the frequency domain, fast Fourier transform (FFT) analysis[31] has identified dynamic baroreflex properties under such noisy condition, but requires longer data segments to cancel the background noise and to identify the dynamic properties with low-frequency band,[38] indicating difficulties to extract short-term changes. In

Address correspondence to Koji Kashihara, Hypertension and Stroke Research Laboratory, Royal North Shore Hospital, University of Sydney, Ground Floor, Building 10, Royal North Shore Hospital, St. Leonards, NSW 2065, Australia. Electronic mail: kojikasi-nils@umin.ac.jp

the spontaneous baroreflex method, the analytical time window based on short-time FFT[5] (STFFT) has been adjusted to evaluate the time-varying gain around the operating point. However, this method may not be suitable for the evaluation of short-term changes in baroreflex properties for AP regulation through sympathetic as well as vagal nerves, at multiple pressure points with background noise. A combination of time and frequency analysis using wavelet transform may be able to identify the dynamic baroreflex properties efficiently regardless of background noise[2,4] by virtue of its high temporal resolution.[34] If dynamic and static characteristics in cardiovascular patients with unstable hemodynamics can be identified in a short-duration baroreflex test, various pathophysiological characteristics may be gained simultaneously.

The first purpose of this study was to examine whether a proposed wavelet-based time-frequency analysis was able to identify the dynamic as well as static baroreflex properties in animals from transient step pressure inputs with background noise during a short-duration test. Next, the proposed analysis was applied to identify unknown dynamic baroreflex properties in nonlinear AP input ranges during the Bezold-Jarisch reflex (BJR). We hypothesized that the proposed analysis could evaluate the baroreflex transfer properties from a short-term protocol, simultaneously at various pressure inputs under normal and BJR conditions. Finally, we examined the possibility of applying the new analysis to human studies to evaluate the dynamic baroreflex for AP regulation through the sympathovagal activity.

METHODS

Pathways of Baroreflex Functions

Under the carotid sinus open-loop condition, we defined the total loop as the system from carotid sinus pressure (CSP) input to AP output, which is divided into the neural arc as the subsystem from CSP input to renal sympathetic nerve activities (RSNA) output and the peripheral arc as the subsystem from RSNA input to AP output.[15] The cardiac baroreflex was defined as the system from CSP to heart rate (HR) response,[52] which may represent sympathovagal control of the heart through the baroreflex.

Surgical Preparations

Animals were cared for in accordance with the *Guiding Principles for the Care and Use of Animals in the Field of Physiological Sciences* approved by the Physiological Society of Japan. Japanese white rabbits were anesthetized with an intravenous injection (2 mL/kg) of a mixture of urethane (250 mg/mL) and α-chloralose (40 mg/mL) followed by a continuous administration (0.2–0.3 mL/kg/h, i.v.). The rabbits were artificially ventilated with oxygen-enriched room air at 0.6 Hz. Raw wave of AP was measured from the right femoral artery, using a high-fidelity pressure transducer (Millar Instruments, Houston, TX). A double-lumen catheter was placed into the right femoral vein for drug administration. The aortic depressor nerves identified by arterial pulse-synchronous activities were sectioned, while bilateral vagi were kept intact. Bilateral carotid sinuses were isolated from the systemic circulation by ligating the external and internal carotid arteries, and were filled with warm physiological saline through catheters inserted into the common carotid arteries. CSP was adjusted with a servo-controlled piston pump controlled by a computer system.

The left renal sympathetic nerve was exposed and a pair of stainless steel wire electrodes (Bioflex wire AS633, Cooner Wire) was attached. The nerve fibers distal to the electrodes were crushed by tight ligature to eliminate afferent signals from the kidney, and were covered in silicone gel (Semicosil 932A/B, Wacker Silicones). The preamplified nerve signal, band-pass filtered at 150–1000 Hz, was full-wave rectified and low-pass filtered at a cutoff frequency of 30 Hz (i.e. Op-amp RC integrator) to quantify nerve activity. Pancuronium bromide (0.3 mg/kg, i.v.) was administered to prevent muscular activity. The body temperature was kept at 38 °C.

Step Input Protocol

The carotid sinus baroreflex negative feedback loop was closed by adjusting CSP to AP level for 20 min after the surgical preparations (8 rabbits weighing 2.7–3.0 kg). The feedback loop was then opened and CSP was maintained at 40 mmHg for 4 min until the AP response reached a steady state. CSP was then increased from 40 to 160 mmHg in increments of 20 mmHg every minute (CSP_{40-60}, CSP_{60-80}, CSP_{80-100}, $CSP_{100-120}$, $CSP_{120-140}$, and $CSP_{140-160}$ changes). The single trial was repeated three times every rabbit. Data were sampled at 200 Hz and were averaged every 40 points for analysis (i.e. pulsatile AP signals were averaged every 0.2 s). HR (beats/min) was counted from the pulse waves of raw AP signals, which are well known as waves synchronized with ECG.[33] RSNA data of each animal were presented in arbitrary units (a.u.), with 1-min averaged background noise taken as zero level and 10-s averaged RSNA at CSP of 40 mmHg in normal condition set as unity.

Data Analysis

Identification of Dynamic Baroreflex

After the recorded data (three times) of CSP, RSNA, AP and HR were averaged in each animal, the signals were convoluted by complex Morlet wavelet, $w(t, f_0)$:[48,49]

$$w(t, f_0) = \frac{1}{\sqrt{\sigma_t\sqrt{\pi}}} \cdot \exp\left(\frac{-t^2}{2\sigma_t^2}\right) \cdot \exp(2\pi f_0 it) \qquad (1)$$

where the $(\sigma_t\sqrt{\pi})^{-1/2}$ normalizes the wavelets to be unity total energy, and the $\exp(-t^2/2\sigma_t^2)$ is a Gaussian shape with the central frequency f_0 at time t. The standard deviation (σ_t) of the time domain is inversely proportional to the standard deviation (σ_f) of the frequency domain [$\sigma_f = (2\pi\sigma_t)^{-1}$]. A constant ratio, f_0/σ_f, determines the effective number of oscillation cycles in the wavelet. The f_0/σ_f was determined[11] as 5 with f_0 ranging from 0.04 to 0.4 Hz[32] in increments of 0.01 Hz. Because the dynamic baroreflex function was well characterized by the transfer function up to around 0.4 Hz based on the corner frequency and slope of gain change,[15,32] the upper frequency limit for analysis was set at 0.4 Hz, considering also the limitation of the step input (low power in high frequency components) and the respiratory frequency of 0.6 Hz. The wavelet duration ($2\sigma_t$) is 39.8 s at 0.04 Hz and 3.98 s at 0.4 Hz, and the spectral band width ($2\sigma_f$) is 0.016 Hz at 0.04 Hz and 0.16 Hz at 0.4 Hz.

The linear trend was subtracted only in animal study, and the continuous wavelet transform of time series $u(t)$ was calculated as the convolution of a complex wavelet [$w(t, f_0)$] with the $u(t)$:

$$\tilde{u}(t, f_0) = w(t, f_0) * u(t) \qquad (2)$$

The power $P(t, f_0)$ of the signal in a frequency band at around f_0 is the squared norm of the wavelet transform: $P(t, f_0) = |\tilde{u}(t, f_0)|^2$. The symbol (*) shows the convolution in the time domain

To identify the dynamic baroreflex property from time-sequential data, we define the transfer function [$H(t, f_0)$] from input to output using wavelet transform as follows.

$$H(t, f_0) = \frac{P_{xy}(t, f_0)}{P_{xx}(t_{\text{event}}, f_0)} \qquad (3)$$

where

$$\begin{cases} P_{xx}(t_{\text{event}}, f_0) = \tilde{x}(t_{\text{event}}, f_0) \cdot \tilde{x}^{\oplus}(t_{\text{event}}, f_0) \\ P_{xy}(t, f_0) = \tilde{x}(t_{\text{event}}, f_0) \cdot \tilde{y}^{\oplus}(t, f_0) \end{cases}$$

$P_{xx}(t_{\text{event}}, f_0)$ is the auto-wavelet spectrum of the input signal [$x(t)$] with central frequency f_0 at a fixed time t_{event} when the power is maximum. The t_{event} shows the sole value of the analysis time (t) at f_0; the transfer function shows the effect of the maximum input power at t_{event} on the output responses during analysis time, t, for every f_0. Here, we used the fixed input value to extract the dynamics strictly against the step input. The cross-wavelet spectrum, $P_{xy}(t, f_0)$, which is an effective way to detect large-amplitude time-localized events,[26] is the convolution of the wavelet transform values of the input-output signals [$\tilde{x}(t_{\text{event}}, f_0)$ and $\tilde{y}^{\oplus}(t, f_0)$]. $\tilde{x}^{\oplus}(t_{\text{event}}, f_0)$ and $\tilde{y}^{\oplus}(t, f_0)$ is the complex conjugate of $x(t_{\text{event}}, f_0)$ and $y(t, f_0)$. The segment for wavelet transform analysis was set at ±30 s of the time of the step input change and was moved to the next area of the step input. The symbol (·) shows the product in the frequency domain, which corresponds to the convolution in the time domain.

To visualize the time-series transfer function during the analysis time (t), the dynamic gain $[|H(t, f_0)| = \sqrt{H_{\text{Re}}(t, f_0)^2 + H_{\text{Im}}(t, f_0)^2}$, where $H_{\text{Re}}(t, f_0)$ and $H_{\text{Im}}(t, f_0)$ are the real and imaginary parts of $H(t, f_0)$] and phase $\left[\varphi(t, f_0) = \tan^{-1}\frac{H_{\text{Im}}(t, f_0)}{H_{\text{Re}}(t, f_0)}\right]$ of the transient transfer function during analysis time were calculated from Eq. (3).

Next, we constructed the bode plot using the maximum dynamic gains, which reflects the maximum values of input and output powers. The phase of Eq. (3) is based on the maximum $P_{xx}(t_{\text{event}}, f_0)$ as the auto-wavelet spectrum of the input signal without the lag time of system response. To calculate the phase of the bode plot, we estimated the lag time of the system response as follows:

$$\hat{L} = t_{P_{xy}\max} - t_{P_{xx}\max}, \qquad (4)$$

where $\hat{L}$ is the mean value between 0.35 and 0.4 Hz of f_0. The data between 0.35 and 0.4 Hz (5 points) were averaged because of the varied estimation. The analysis time was set to 0–6 s and the phase unwrap process to make it continuous across 2π phase discontinuities by adding multiples of $\pm 2\pi$ was applied. $t_{P_{xx}\max}$ is the time at the maximum auto power spectrum of the input data; $t_{P_{xy}\max}$ is the time at the maximum cross power spectrum of input-output data. Using the estimated lag time (L) of the system response, the phase [$\varphi(t_{\max}, f_0)$] of the transient transfer function is shown as follows:

$$\varphi(t_{\max}, f_0) = \tan^{-1}\frac{H'_{\text{Im}}(t_{\max}, f_0)}{H'_{\text{Re}}(t_{\max}, f_0)} \qquad (5)$$

where

$$H'(t_{\max}, f_0) = H(t_{\max}, f_0) \cdot \exp(-2\pi f_0 iL)$$

$H'_{Re}(t_{max}, f_0)$ and $H'_{Im}(t_{max}, f_0)$ are the real and imaginary parts of $H'(t_{max}, f_0)$ with lag time, L. t_{max} is the time when the dynamic gain is maximum.

Static Characteristics

After the RSNA, AP, and HR during the last 10 s of each CSP level were averaged using the data of the step-input protocol, the static characteristics of total baroreflex loop, neural arc, and cardiac baroreflex control were examined by regression analysis for the logistic function.[24,46,47] To quantify static characteristics of the peripheral arc, linear regression analysis was performed. The closed-loop operating point of the baroreflex (AP_{OP}) was determined from the intersection point between the CSP-AP curve (total baroreflex loop) and CSP-AP identity line. AP_{OP} was also determined from AP at the intersection point between the CSP-RSNA curve (neural arc) and RSNA-AP line (peripheral arc) in the equilibrium diagram.[18]

Standard Analysis

The STFFT as a traditional time-frequency method was applied to the step-input (±20 mmHg) protocol, using the model response between CSP and AP (see Appendix). The time window was set to 12.8 s (64 data points) and 51.2 s (256 points, which is close to that at the lowest frequency in the used wavelet method). After the application of the detrend and Hanning window, power spectral densities of the CSP and AP and the transfer gain of the cross-spectra were computed every 200 ms. In the STFFT (256 points), pseudo-random noises were added to the input (within ±0.1 mmHg) and output (±1 mmHg every 200 ms) signals. The STFFT analysis was also compared with the proposed wavelet analysis over frequencies under the pseudo-random noise within ±0.1 mmHg in the input and ±1 or ±2 mmHg in output every 200 ms.

Experiment of Bezold-Jarisch Reflex

To elucidate the modified wavelet-based analysis in the pathophysiological condition, the previous datasets assessing static baroreflex during BJR[18] were reanalyzed; the data at sampling rate of 200 Hz were averaged every 40 points. In 8 anesthetized rabbits with sectioned aortic depressor nerves, intact vagi, and isolated carotid sinuses, CSP was increased stepwise while AP and HR were recorded before and after 7-min administration of a serotonin ($5\text{-}HT_3$) receptor agonist, phenylbiguanide (PBG, 100 μg/kg/min, intravenous infusion): Control and PBG conditions. Vagal afferent was confirmed as the main pathway of the BJR induced by intravenous PBG infusion.[20]

Cardiac Baroreflex

The role of cardiac baroreflex (CSP to HR response) was studied, focusing on the contribution of the cardiac sympathovagal activity to dynamic baroreflex for AP regulation. The ratio of the transfer functions between cardiac baroreflex and total (CSP-AP) loop was calculated under Control and PBG conditions, using the results from the proposed analysis.

Statistical Analysis

All data are expressed as mean ± SEM. The gain, power, and frequency in the figures are shown in log scales. The transfer functions in the neural and peripheral arcs were normalized in each animal so that the average gain in all stepwise changes of normal condition became unity at 0.04 Hz. To test the difference among six stepwise changes or between the Control and PBG conditions, we obtained the gain at 0.04 ($G_{0.04}$), the average slope of the gains between 0.1 to 0.4 Hz (Slope), and the lag time in each animal. One-way analysis of variance with multiple comparisons using Bonferroni correction[9] was applied to assess the level differences. Differences were considered statistically significant at $p < 0.05$.

Simulation for Closed-Loop Baroreflex

The carotid sinus open-loop animal experiment should be linked to human closed-loop baroreflex to explore the possibility of applying the proposed analysis to clinical diagnosis. We performed a simulation study, using the emulated cardiac baroreflex model from observed AP input to observed HR output under the closed-loop AP response (see Appendix) to test the accuracy of the proposed wavelet-based analysis and to acquire the transfer functions of the cardiac baroreflex for use in human laboratory test.

RESULTS

Test of Wavelet Analysis

The proposed wavelet-based analysis was tested using the baroreflex model response between CSP and AP under carotid sinus open-loop condition (see Appendix). After the calculation of the wavelet power spectrum for the input and the input-output cross spectrum (Fig. 2a), the transfer function was acquired (Fig. 2b). The gains reached the maximum immediately after the step input at 60 s and the phase changed greatly when approaching the maximum gain. Bode plots were extracted from the maximum points of the time-course transfer function with and without

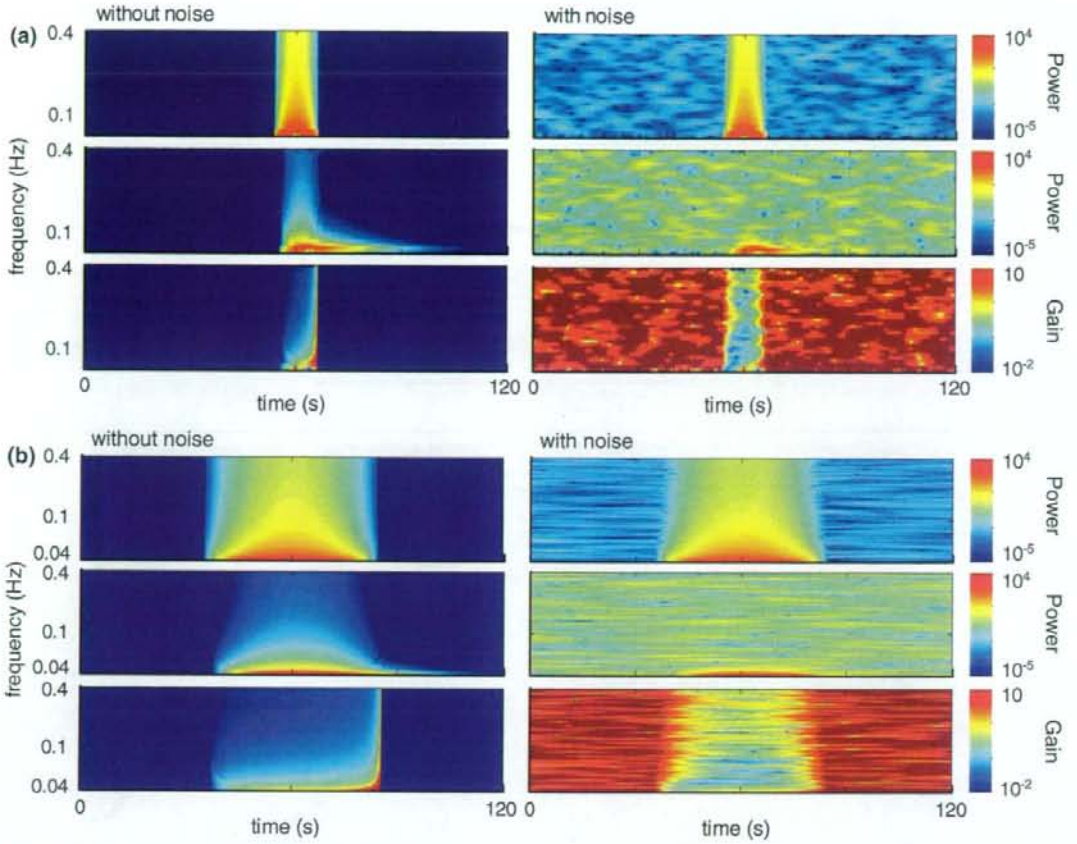

FIGURE 1. Time-frequency method based on the short-time FFT for system identification using the simulated step-input protocol. Time windows, 12.8 s (a) and 51.2 s (b). Power spectral densities of carotid sinus pressure (CSP) input (*top*) and arterial pressure (AP) output (*middle*) and transfer gain (*bottom*) in the absence (*left*) or presence (*right*) of pseudo-random noises.

background noise (Fig. 2c). In the presence of pseudo-random noise (within ±0.01 mmHg in input and ±1 mmHg in output changed every 200 ms), the transfer function closely resembled the theoretical values. Compared to the STFFT (Fig. 1), the proposed wavelet method could accurately estimate the transfer function over different frequencies, regardless of a poor signal to noise (S/N) ratio at higher frequency, because of the property of the step input power (Fig. 2d).

Dynamic Baroreflex

The averaged RSNA, AP, and HR responses to the step-input changes were decreased with the increments in CSP from 40 to 160 mmHg every minute ($n = 8$, Fig. 3a). In the averaged time series ($n = 8$, Fig. 3b), the power spectrums at all step inputs were the same values at each frequency level because of a constant change of +20 mmHg (greater in low frequency and smaller in high frequency). The powers of RSNA, AP, and HR change were higher at CSP_{80-100} than other CSP changes over all frequency ranges, and the magnitudes were especially small at low or high CSP changes.

The averaged ($n = 8$) time series of transfer functions in the neural arc (a), peripheral arc (b), total loop (c) and cardiac baroreflex (d) were calculated after wavelet transform (Fig. 4). In the neural arc, gain values in low frequencies were much less at CSP changes away from the operating point. In the peripheral arc, low pass characteristics in the gains were observed at all CSP changes except the lowest CSP_{40-60} change reflecting spontaneous neural firing. In the total baroreflex loop, the gains at CSP changes within 60–120 mmHg were higher than those at other CSP changes, indicating low-pass characteristics. In the cardiac baroreflex, the gains were smaller at the

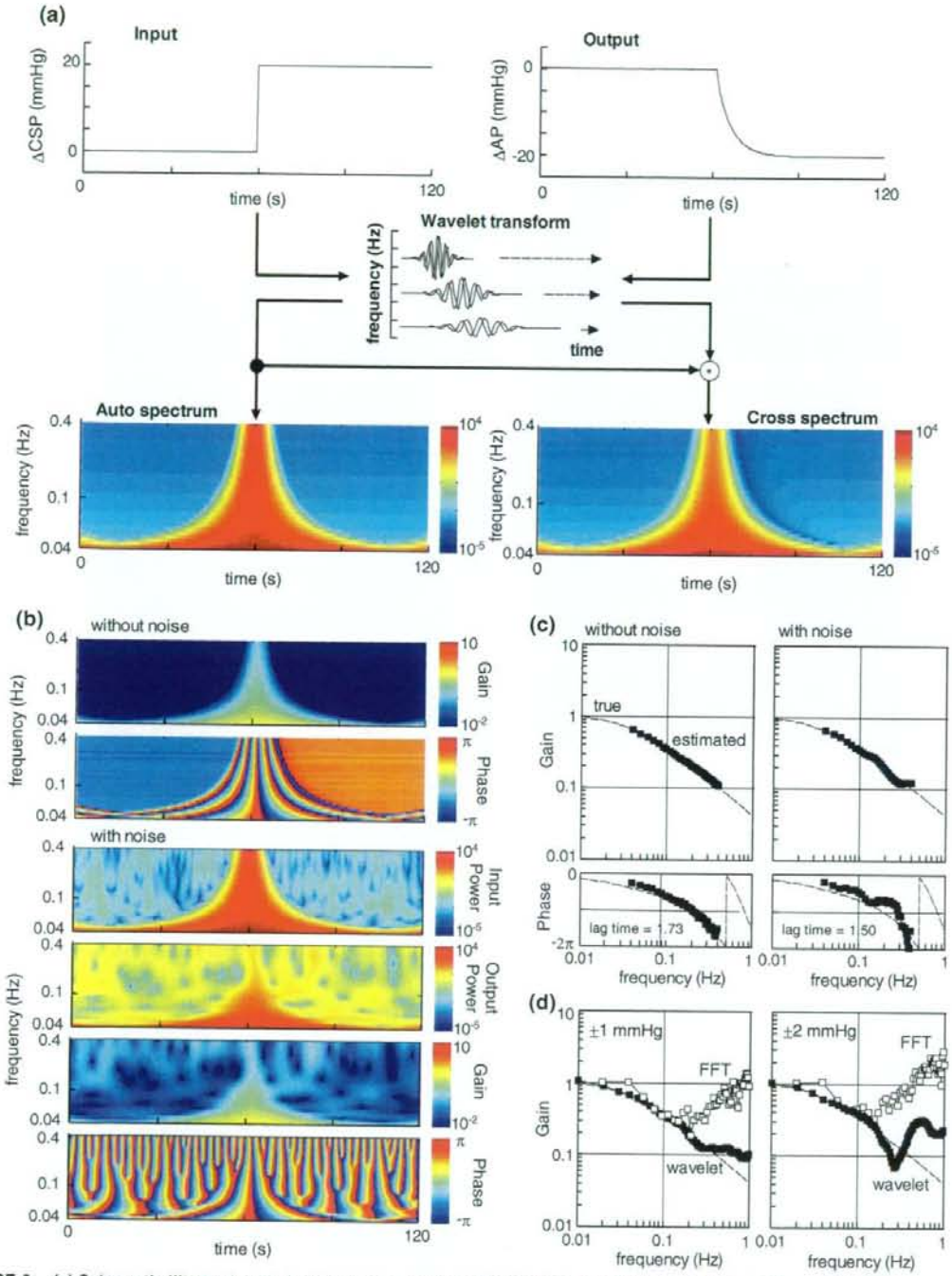

FIGURE 2. (a) Schematic illustration of the time-course system identification using wavelet analysis. The model response of total loop from CSP to AP under the carotid sinus open-loop condition was assessed for 120 s. Step input change of 20 mmHg was added to the system at 60 s. The time-series transfer function estimated by our wavelet analysis (b) and transfer function extracted from the time-course data of the total loop transfer function and the theoretical data (c). Gain (*top*) and phase (*bottom*) in the absence or presence of pseudo-random noise. (d) Gains in the short-time FFT and proposed wavelet analyses over wide frequencies (0.01–1 Hz) under the pseudo-random noise [±1 mmHg (*left*) and ±2 mmHg (*right*)].

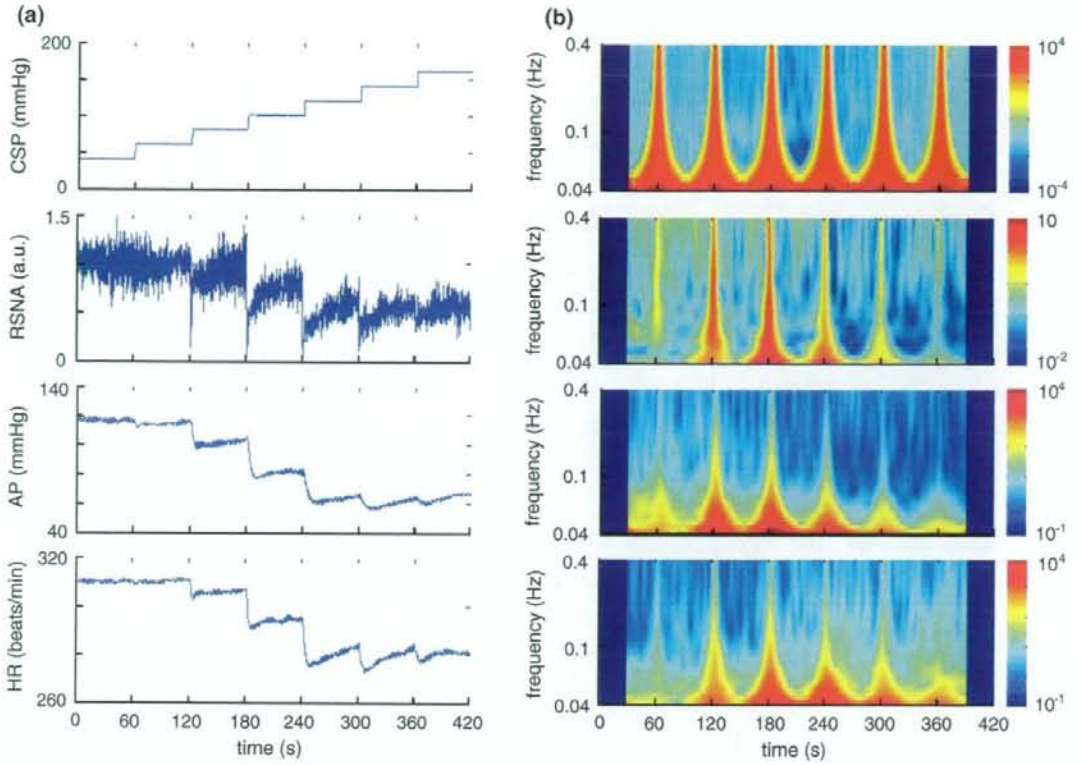

FIGURE 3. Averaged time series (a, $n = 8$) and wavelet power (b, $n = 8$) of CSP, renal sympathetic nerve activities (RSNA), AP, and heart rate (HR) during the static protocol. CSP was increased from 40 to 160 mmHg in 20 mmHg increments, resulting in changes of RSNA, AP, and HR through the carotid sinus baroreflex.

CSP_{40-60} and $CSP_{140-160}$ changes than other CSP changes.

Figure 5 and Table 1 show the average gain and phase ($n = 8$) in the neural arc (a), peripheral arc (b), total loop (c), and cardiac baroreflex (d). In the neural arc, $G_{0.04}$ (2.42 ± 0.07 a.u./mmHg) at the CSP_{80-100} change was the highest among all CSP changes, and was almost four to five times higher than those at the CSP_{40-60} (0.54 ± 0.09, $p < 0.01$) and $CSP_{140-160}$ (0.62 ± 0.06, $p < 0.01$) changes. Slopes increased significantly at lower and higher CSP changes compared with the $CSP_{100-120}$ change. Lag time at CSP_{80-100} was the shortest among all CSP changes. In the peripheral arc, Slope and lag time did not differ significantly among the CSP changes, whereas $G_{0.04}$ showed a tendency to decrease slightly with increase of CSP. In the total baroreflex, $G_{0.04}$ at CSP_{80-100} change (1.28 ± 0.12) was significantly higher compared to other CSP changes. Slopes were significantly greater at CSP changes within 60–120 mmHg than other CSP changes. Lag time did not differ significantly among CSP changes. In the cardiac baroreflex, $G_{0.04}$ (0.90 ± 0.18 and 0.92 ± 0.19 beats/min/mmHg) and Slopes were significantly higher at CSP_{80-100} and $CSP_{100-120}$ changes than other CSP changes. There were no significant differences in lag time among CSP changes.

Static Baroreflex

The static characteristics of the total loop were averaged ($n = 8$). Regression analysis was performed for logistic functions. Response range, coefficient of gain, midpoint of input axis, and minimum value of output were 0.45, 0.11, 99.6, and 0.55 in the neural arc, 65.2, 0.07, 97.6, and 69.4 in the total loop, and 29.5, 0.11, 98.2, and 281.2 in the cardiac baroreflex. Linear regression analysis was performed in the peripheral arc (static gain = 0.0086 and offset pressure = 0.027). The intersection between the CSP-AP curve and the line of identity corresponds to AP_{OP} (94.3 mmHg) located in the steepest portion (80–100 mmHg) of the sigmoid